Title

PERFORMANCE AND MATERIALS ASPECTS OF Ge:Be AND Ge:Ga PHOTOCONDUCTORS FOR FAR INFRARED DETECTION

Author

Haegel, N.M.

Publication Date

1983-09-01

Lawrence Berkeley Laboratory
UNIVERSITY OF CALIFORNIA

Engineering & Technical Services Division

PERFORMANCE AND MATERIALS ASPECTS OF Ge:Be AND Ge:Ga PHOTOCONDUCTORS FOR FAR INFRARED DETECTION

N.M. Haegel
(M.S. Thesis)

September 1983

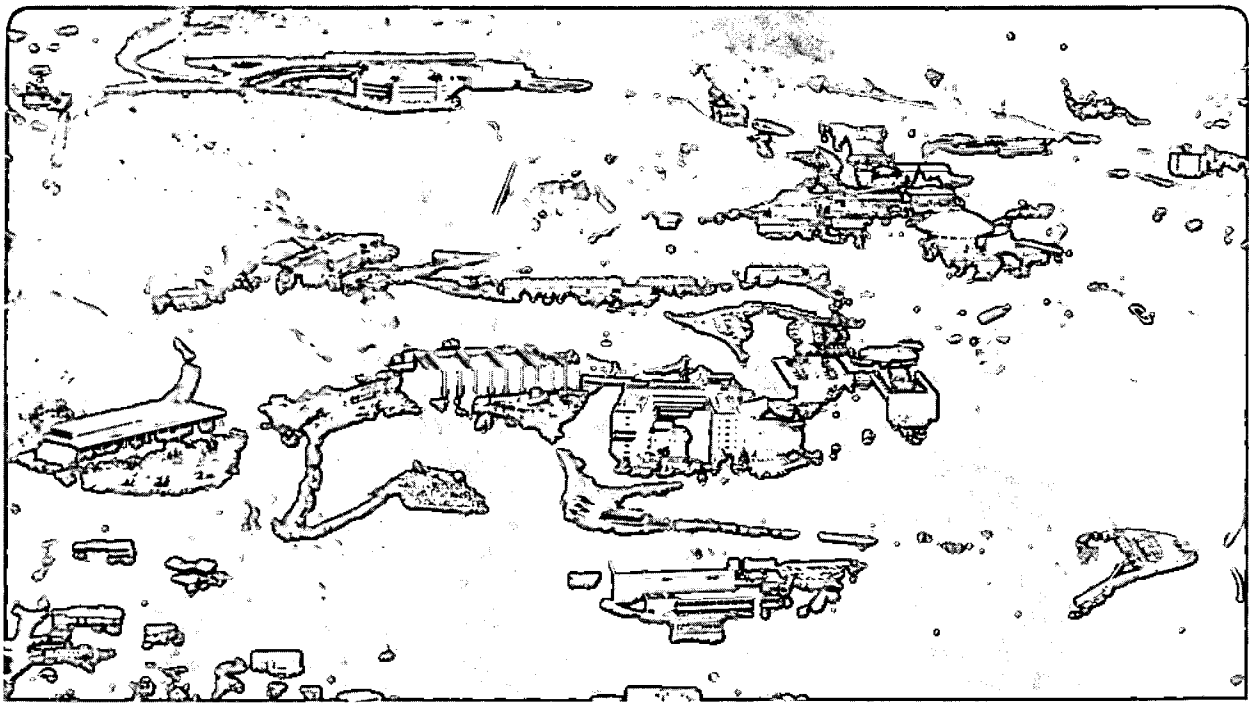

Prepared for the U.S. Department of Energy under Contract DE-AC03-76SF00098

DISCLAIMER

APPENDIX 1 - SIGNAL CALCULATION AND DIFFRACTION ANALYSIS

Consider the following situation and ask: What is the DC photon flux from each of the blackbody sources and what is the chopped signal that reaches the detector?

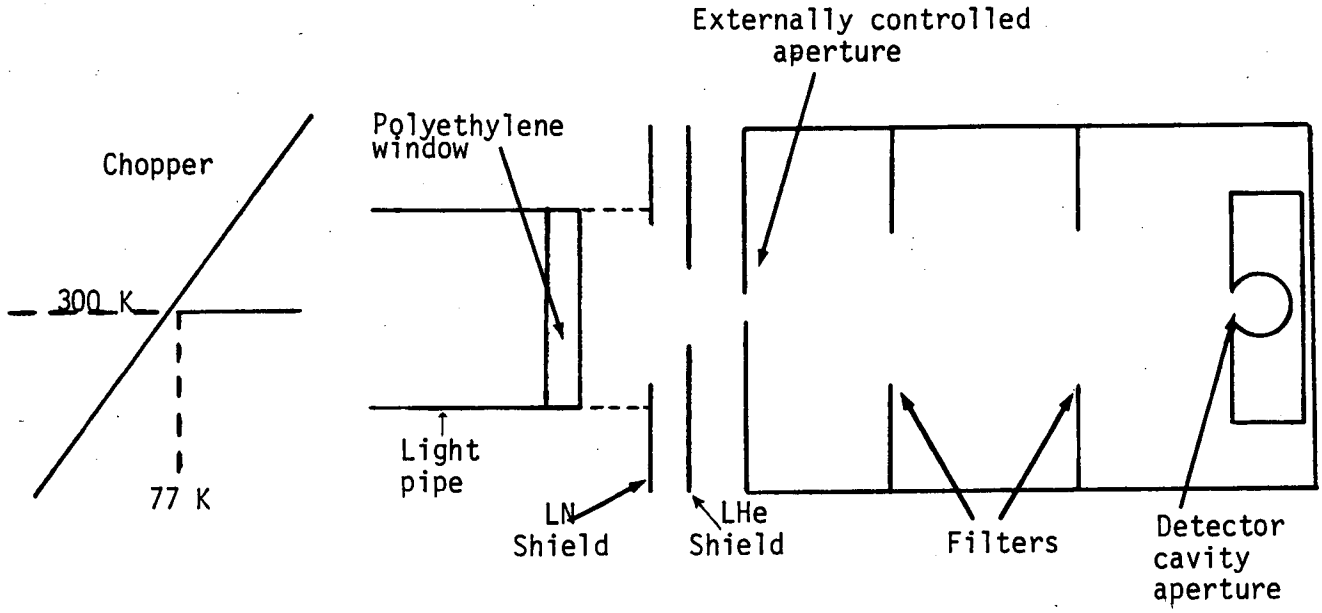

1) Calculate the blackbody radiation from the 300 and 77 K sources.

$$W(\lambda) = \frac{2\pi hc^2}{\lambda^5}\left[e^{\frac{hc}{\lambda kT}} - 1\right]^{-1} \qquad 37$$

$$= \frac{3.74\times10^4}{\lambda^5}\left[e^{\frac{1.44\times10^4}{\lambda T}} - 1\right]^{-1} \qquad \text{for } \lambda(\mu m),\ T(K) \rightarrow W \text{ in Watts/cm}^2/\mu m$$

2) Determine the transmission of the window experimentally.

$\frac{I}{I_o}$ =% transmission measured through the window material.

Given $R + A + T = 1$ and $A \simeq E$.

For polyethylene $n = 1.46$ through far-IR

Since $\epsilon' = n^2 - k^2$, $\epsilon' \approx 2.1 - 2.5 \rightarrow k$ is small

$$R = \rho^2 = \left(\frac{n - 1}{n + 1}\right)^2 = 3\%$$

where R = reflectivity
T = transmissivity
E = emissivity
A = absorptivity

$\therefore$ Neglect R and $A + T = 1$ determines T and E.

3) Calculate the geometric factor, considering purely geometric optics.

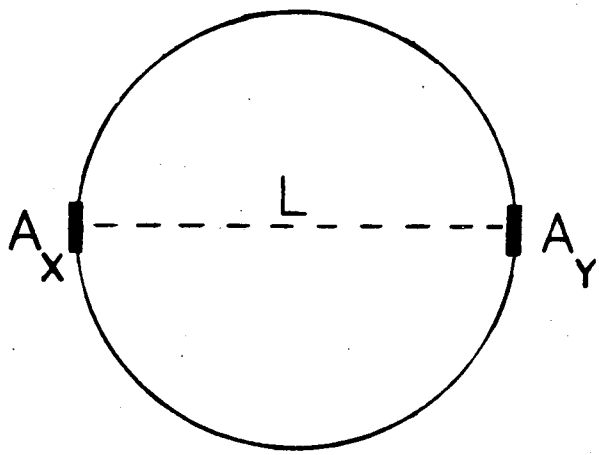

The radiation seen at y due to the source at x is:

$$W_{total} \times \frac{A_x A_y}{\pi L^2}$$

for W in watts/$cm^2/\mu m$ and A_X, A_Y in cm^2, L in cm.

4) The filter trains have characteristic peak transmissions and bandwidths[7] (see Table 1).

T - transmission (peak) in %

Bandwidth (in μm)

LBL-16694

PERFORMANCE AND MATERIALS ASPECTS OF Ge:Be AND Ge:Ga PHOTOCONDUCTORS FOR FAR INFRARED DETECTION

Nancy Marie Haegel
(M.S. Thesis)

Lawrence Berkeley Laboratory
University of California
Berkeley, California 94720

September 1983

ABSTRACT

Ge:Be and Ge:Ga single crystal material has been developed for use as far infrared photoconductors in low photon background applications. Crystal growth and characterization have been performed in conjunction with measurements of photoconductor performance. Reliable Be doping for Ge:Be detectors has been achieved using Czochralski growth from a carbon susceptor under vacuum. These detectors provide higher responsivity and lower noise equivalent power (NEP) than the Ge:Ga detectors currently used in the 30 - 50 μm wavelength range. The responsivity of Ge:Be detectors is strongly temperature dependent when the residual shallow acceptors are closely compensated. The breakdown field in low compensation Ge:Ga detectors ($K = 10^{-4}$) has been extended from 1.0 to 2.0 V/cm by the introduction of neutral scattering centers. In-diffusion of Cu has been used to limit the mobility and allow the detectors to be operated at higher biases where optimum NEP and responsivity are attained.

ACKNOWLEDGEMENTS

I am most grateful to Professor Eugene Haller for his support and supervision and for the generous contribution of time and effort that he has made to all aspects of this work. The photoconductor testing cryostat was built by Paul Luke, LBL staff scientist. His instruction and expertise have been a continuous source of assistance and are gratefully acknowledged. Our group is indebted to Professor Paul Richards and Mark Hueschen for their advice in the design of the test dewar and for the benefit of their experience in the area of infrared detectors. Professor Charles Townes, Dr. Dan Watson, and Dr. Mike Crawford have greatly aided this work by providing us with the necessary filters.

William Hansen, Dick Davis,, Nick Palaio, Dr. Steven Pearton, and Joe Kahn, members of our group at LBL, have contributed to this work extensively with their advice and assistance. I would especially like to thank Bob McMurray for the contributions he has made with his PTIS measurements.

The manuscript and figures have been prepared by Lynne Dory, Sule Ozturkmen, and Kazuo Shimada. Their contributions are gratefully acknowledged.

Finally, I wish to acknowledge the support of a National Science Foundation Fellowship during the past two years. This work has been supported by NASA Contract No. W-14,606 under Interagency Agreement with the Director's Office of Energy Research, Office of Health and Environmental Research, U.S. Department of Energy under Contract No. DE-AC03-76SF00098.

TABLE OF CONTENTS

1. INTRODUCTION

A photoconductor is a device which displays a change in conductivity in response to the absorption of incident radiation. In semiconductors and insulators, incident photons can produce free carriers, thereby changing the conductivity of the material and establishing the photoconductor as a transducer which converts incident radiation into an electrical signal. An intrinsic photoconductor is one in which free carriers, both electrons and holes, are produced by the excitation of an electron across the full band gap into the conduction band, leaving a hole in the valence band. As the name implies, the photoconductive response of these devices is intrinsically dependent upon the electrical properties of the undoped material. When the free carriers are produced from a dominant level within the band gap, a single carrier is transported to one of the bands, leaving behind an ionized defect or impurity level. This type of device is referred to as an extrinsic photoconductor, indicating that the photoconductive response is due to the presence of dopant atoms which are extrinsic to the host lattice.

Extrinsic photoconductors are rapidly gaining importance as detectors of far infrared radiation for astronomy-related space missions. With a wide variety of impurities available for introduction into different semiconductors (primarily Si, Ge and GaAs), detectors can be made which are optimally sensitive to a wide range of wavelengths. Unstressed Ge detectors, for example, are used for the detection of wavelengths ranging from 30 to 120 μm. These detectors are able, under appropriate conditions, to detect small changes in a

photon stream at very low levels (i.e., 10^6 - 10^{10} photons/second) of photon flux.

Much of the early work on extrinsic photoconductors was done in the 1950's and 1960's[1]. Recently, however, advances in material and device fabrication processes, as well as the demand from the astronomy community for increasingly sensitive detectors, has led to a renewed interest in the study and development of these devices. The successful launch and operation of the Infrared Astronomical Satellite (IRAS) has focused attention on the opportunities for observation now available on orbiting satellites which eliminate the problem of atmospheric background and absorption.

The objective of this work was the development of Ge:Ga and Ge:Be single crystals for use as far-infrared photoconductors and the evaluation of their photoconductive behavior. The effects of materials parameters such as doping concentration and compensation were studied in order to optimize detector performance. Research and development of Ge:Be detectors was undertaken to meet the need for optimized detectors in the 30 - 50 μm wavelength range. Early stages of detector development required the establishment of controlled crystal growth conditions for this material, characterization of the material, and extensive testing of prototype detectors. In Ge:Ga, the degree of compensation has previously been established as an important detector parameter. Detectors fabricated from low compensation material have the potential to provide increased signal output per watt of incident photon power if certain noise and breakdown problems can be overcome. This was the objective of low compensation material development and detector evaluation of Ge:Ga.

1.1 Mechanisms of Extrinsic Photoconductivity

The photoconductive effect in extrinsically doped Ge is observed when infrared photons are absorbed and neutral impurities are ionized to create free carriers. For acceptors, such as Ga or Be, the energy of the photon absorbed must be sufficient to free the hole which is bound by the Coulomb potential of the fixed negatively charged acceptor site. The photoionization of the neutral acceptor excites the hole into the valence band, where it is free to travel through the lattice and contribute to the conductivity. In extrinsic Ge photoconductors for far infrared detection, the dopant atoms have small (i.e., < 30 meV) ionization energies. These levels are completely thermally ionized at both room temperature and liquid nitrogen temperature, hence liquid helium temperatures are required to keep the acceptor sites neutral and available for photoionization.

The relationship between ionization energy and threshold wavelength is:

$$E_i = \frac{hc}{\lambda} = \frac{1240}{\lambda}$$

where E_i = ionization energy in meV and λ = related wavelength in μm. Over a larger energy spectrum, one generally observes that the absorption of photons, and subsequently the photoconductive response $\Delta\sigma$, has a threshold, followed by a peak response, and then a decrease in photoconductivity with increasing photon energy. This is shown schematically in Fig. 1. Such curves are known as the "spectral response" of a given dopant species.

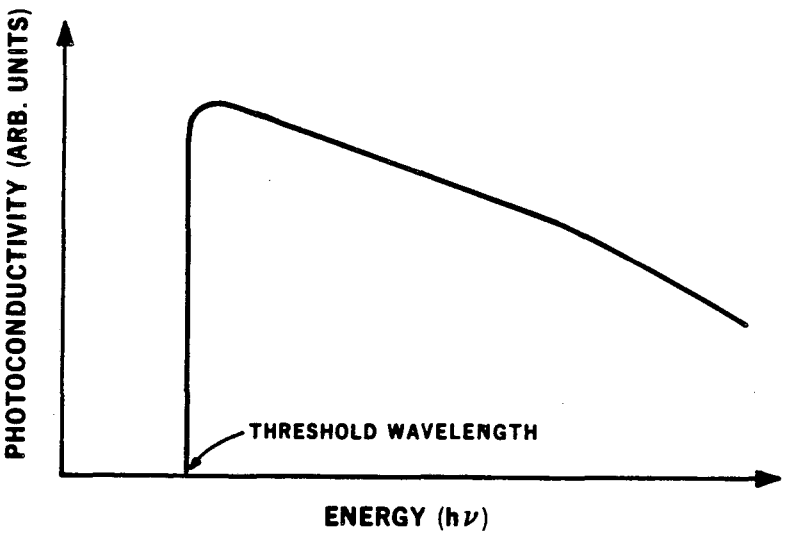

XBL 837-10819

Fig. 1. Schematic photoconductive power response as a function of photon energy (photon power held constant).

The shape of the spectral response curve is understood physically in terms of the probability of electric dipole transitions between the bound state and available continuum states[2]. The location of the peak spectral response is directly related to the ground state energy of the primary dopant. The ionization energies of many impurities in Ge have been well characterized, both optically and thermally. Within the limits imposed by these ionization energies, then, detectors can be designed which have an optimum spectral response in a given wavelength region.

Once a hole is excited into the valence band, its contribution to a change in conductivity of the detector will depend upon the distance it moves through the lattice and the time before it returns to the ground state of another ionized impurity. The latter parameter, known

as carrier lifetime, is of critical importance to both the speed and the magnitude of the photoconductive response. One generally defines two types of lifetime: the "excited lifetime" which is the total time from the creation of the carrier until its recombination into a bound state, and the "free lifetime" which is the time during which the carrier is free (i.e., untrapped) and can contribute to conduction[3].

Much of the early work done on photoconductivity involved intrinsic materials, and so trapping and recombination centers were defined for systems with both electrons and holes. In extrinsic semiconductors, however, conduction is usually assumed to be dominated by a single type of carrier. This assumption is especially valid in the cases considered here, i.e., Ge:Ga and Ge:Be at < 4.2 K, where there are no electron-hole pairs produced by thermal excitation and optical excitation is fully suppressed by appropriate filters. In systems such as these, trapping is associated primarily with the excited states of ionized acceptor sites, as well as with other possible crystalline or impurity defects in the crystal. Recombination is the process by which a free hole recombines into the ground state of an A^- site, converting it again into a neutral center.

The motion of a free carrier in the lattice is characterized by its mobility. Lattice disturbances, such as vibrations, dislocations, impurities, etc., cause scattering of free carriers and limit their mobility. The three primary mechanisms which control mobility in an extrinsic photoconductor are lattice scattering (also called phonon scattering), charged impurity scattering, and neutral impurity scattering. Determining which mechanism is dominant in a given application depends on the dopant concentration, the degree of compensation,

and the temperature. Scattering from lattice vibrations in p-type Ge at T < 70 K has a temperature dependence[4] of $T^{-3/2}$. At T = 4.2 K, with the dopant concentrations in the range of 10^{14} to 10^{15} cm^{-3} for typical extrinsic Ge photoconductors, the lattice effect is small compared to the scattering from either charged or neutral impurities. Dopant concentrations and compensation, then, are the primary materials parameters affecting photoconductive response because they determine both the mobility and the lifetime.

1.2 Detector Parameters

The combined effect of photon absorption, carrier lifetime, and carrier mobility results in a certain magnitude change in conductivity for a given signal of incident photons. To express this result quantitatively, several detector parameters are defined which encompass all these effects and provide a basis for the comparison of detector performance. These parameters characterize the size of the signal and the signal-to-noise ratio of an operating detector.

A modulated signal of incoming photons, as shown in Fig. 2, will produce a corresponding change in the conductivity of the detector. The responsivity is a measure of this change and is defined as the signal output per watt of signal input. The change in conductivity (or resistivity) is usually determined by measuring the change in current through the detector at a fixed bias. Responsivity, then, is normally expressed in terms of Amperes/Watt. In terms of detector parameters, the responsivity is:

$$R = \frac{h\nu}{e} G_n$$

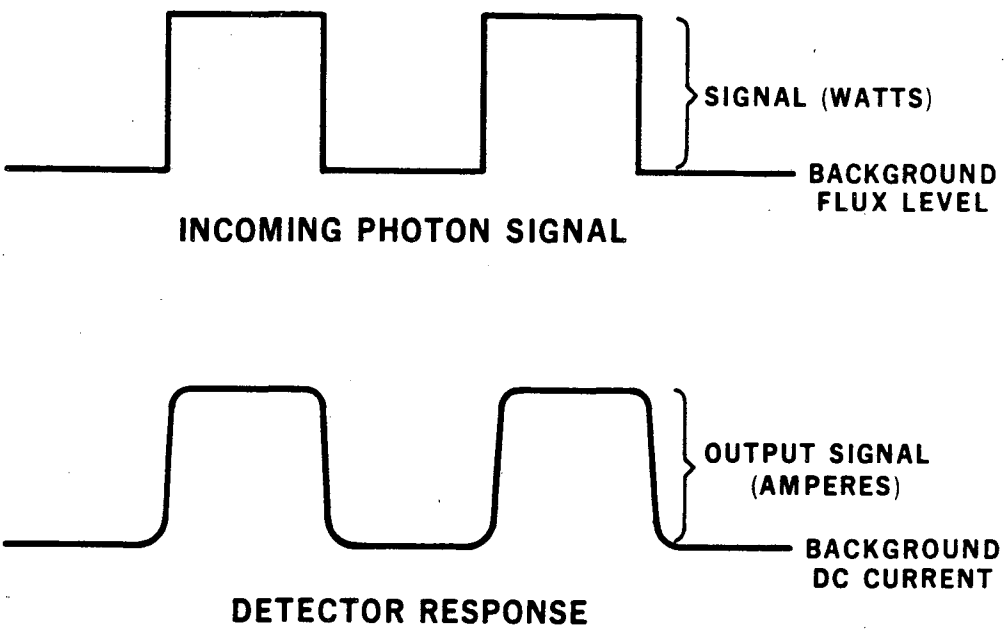

Fig. 2. Incoming signal and detector response.

where $h\nu/e$ = photon energy/Coulomb; G = carriers detected/carriers produced; and η = carriers produced/photons incident. The dimensionless parameter associated with responsivity is the "gain-quantum efficiency", $G\eta$. The gain, G, is best defined as the ratio of free carrier lifetime, τ, to the transit time, t, for a carrier moving under a given bias across a detector of defined dimension. Since the transit time is v_{drift}/length, one can write:

$$G = \frac{\tau}{t} = \tau\mu\frac{V}{L^2}$$

In its simplest form, then, gain is dependent upon the detector size, as well as upon the critical parameters of lifetime and mobility.

The responsive quantum efficiency, η, is defined as the ratio of the number of photons absorbed in the detector to the number of photons incident upon it. In many experimental situations, and for all the results to be presented here, the detector is enclosed in an "integrating cavity" to assure a high quantum efficiency. A polished metal cavity, for example, will reflect infrared photons which may be either reflected from the detector surface or transmitted through the detector without being absorbed. Since a large quantum efficiency is necessary for optimum responsivity, an integrating cavity provides the mechanism for multiple passes and optimum absorption.

The signal-to-noise ratio is the most important parameter which characterizes the performance of a photoconductor. Considering the detector alone, apart from its associated electronics, there are four primary sources of noise to be considered:

1. noise from the thermal generation and associated recombination of free carriers,
2. noise from the photon generation and associated recombination of free carriers,
3. 1/f noise, which is usually associated with contacts or surface effects, and
4. Johnson noise of the resistive load[5].

The noise equivalent power, NEP, is defined as the power required to produce a signal-to-noise ratio of one per unit bandwidth. Experimentally, then:

$$NEP = \frac{P}{S/N}$$

where P = signal power (W); S = signal ($A/\sqrt{Hz}$ or $V/\sqrt{Hz}$); and N = background noise ($A/\sqrt{Hz}$ or $V/\sqrt{Hz}$). Background refers to the constant photon flux which the detector sees in the absence of any signal.

In low temperature photoconductor applications, the dominant noise source is either the noise associated with the random arrival of photons in the photon stream or the Johnson noise of the feedback resistor. Thermal generation is minimal at the optimum detector operating temperature, and 1/f noise can be reduced with appropriate contact and fabrication technology. Under low backgrounds or at low bias across the detector, the Johnson noise can determine the noise voltage and establish the detection limit of the photoconductor. At higher background, or with increased photoconductive gain, photon noise can dominate, and the detector mode of operation is referred to as background limited.

For an average background power P, provided by a thermal radiator, it has been shown that the fluctuation in the photon stream per unit time[6] is given by:

$$\overline{P_\Delta^2} = \frac{2h\nu P}{1 - e^{-h\nu/kT}}$$

where $h\nu$ = photon energy and T_B = background temperature. Fluctuations exist even in steady streams of thermal radiation. In many detector applications, the low background temperature and the wavelengths of interest are such that $h\nu >> kT_B$. In this case, the Bose-Einstein statistics approach a Poisson distribution, and:

$$\overline{P_\Delta^2} = 2h\nu P$$

The validity of this approximation must be checked for each application. In the Poisson limit, then, the photon signal required to match the noise voltage associated with photon fluctuations will be:

$$P_S = (2Ph\nu B)^{\frac{1}{2}}$$

where B ≡ bandwidth. Since all photons in an incident signal are not necessarily absorbed, due to reflection or transmission, an efficiency factor η is introduced and:

$$P_S = 2\left(\frac{Ph\nu B}{\eta}\right)^{\frac{1}{2}}$$

$$\text{or NEP}_{\substack{\text{Background} \\ \text{limited}}} = 2\left(\frac{Ph\nu}{\eta}\right)^{\frac{1}{2}} \quad \text{in } W/\sqrt{Hz}$$

The ratio of the experimental and the background limited NEP is often used as a criterion for detector performance. Using this approach, any excess noise, whether from electronics or contacts or any other source, is reflected as a low quantum efficiency η. Since these effects are clearly unrelated to the efficiency of photon absorption, η, in the NEP expression is usually referred to as a detective quantum efficiency. For a detector in an integrating cavity, one often assumes a responsive quantum efficiency of one and calculates a detective quantum efficiency, $\eta_{detective}$, from the relationship:

$$\frac{NEP_{\text{Background limited}}}{NEP_{\text{Experimental}}} = \frac{2(Ph\nu)^{\frac{1}{2}}}{2\left(\frac{Ph\nu}{\eta_{detective}}\right)^{\frac{1}{2}}}$$

so that $\eta_{detective} = \left(\frac{NEP_{Background\ limited}}{NEP_{experimental}}\right)^2$. In this case, $\eta_{detective}$ is a measure of the signal-to-noise performance of the detector relative to the ideal NEP.

2. EXPERIMENTAL PROCEDURES

2.1 Test Apparatus

The experimental approach to this project involved an interaction between materials development and characterization and detector evaluation. Procedures related to materials development and characterization will be described in detail for specific applications. At this point, however, some statements can be made about detector testing procedures which are applicable to all the results to be presented.

The objective of the detector evaluation was to obtain information about the performance of detector materials under conditions which simulate the conditions of intended use. Since the primary application in infrared astronomy is for conditions of low background (10^6 - 10^{10} photons/second), the most stringent testing requirement was that an accurate estimate of the photon signal be made and that stray radiation be eliminated from the detector environment. In addition, as previously mentioned, extrinsic Ge detectors must be operated near 4.2 K.

The dewar used for photoconductor testing is shown in Figs. 3 and 4. It was obtained from Infrared Laboratories (Model HD3), Tucson, Arizona. A liquid helium space with a volume of approximately 1 liter is shielded with a liquid nitrogen jacket. A common vacuum space provides both thermal insulation and an evacuated space for the detector. The working area is a thick copper plate which is in contact with the liquid helium bath. The detector, its cavity, and all its surroundings are heat sunk directly to this plate, with pure indium foil.

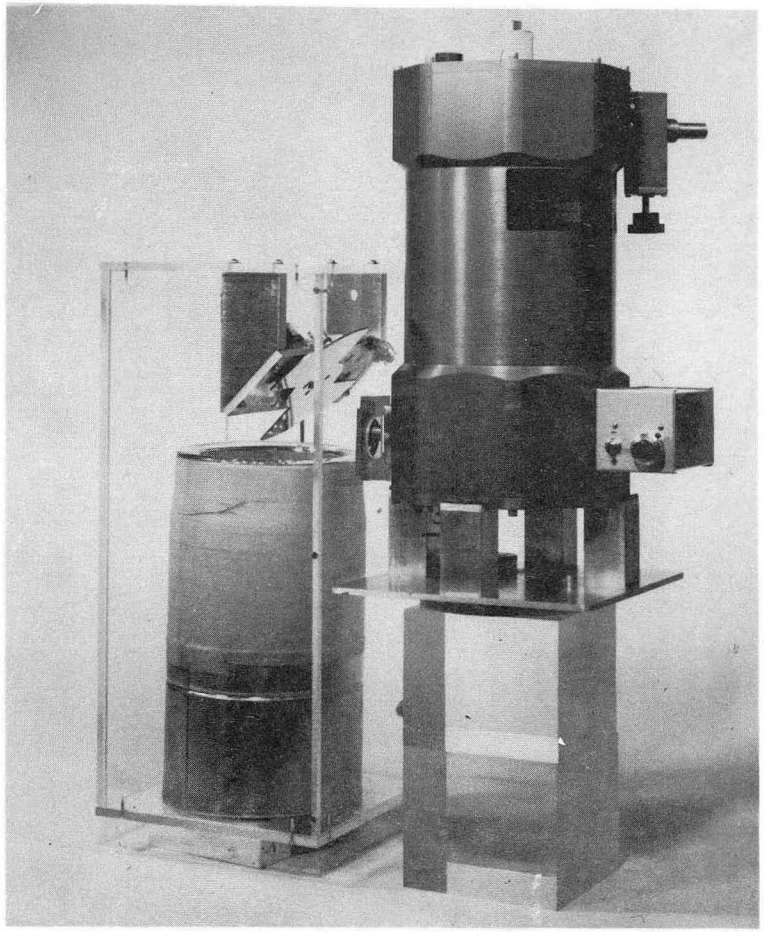

CBB 817-6972

Fig. 3. Photoconductor test dewar and chopper.

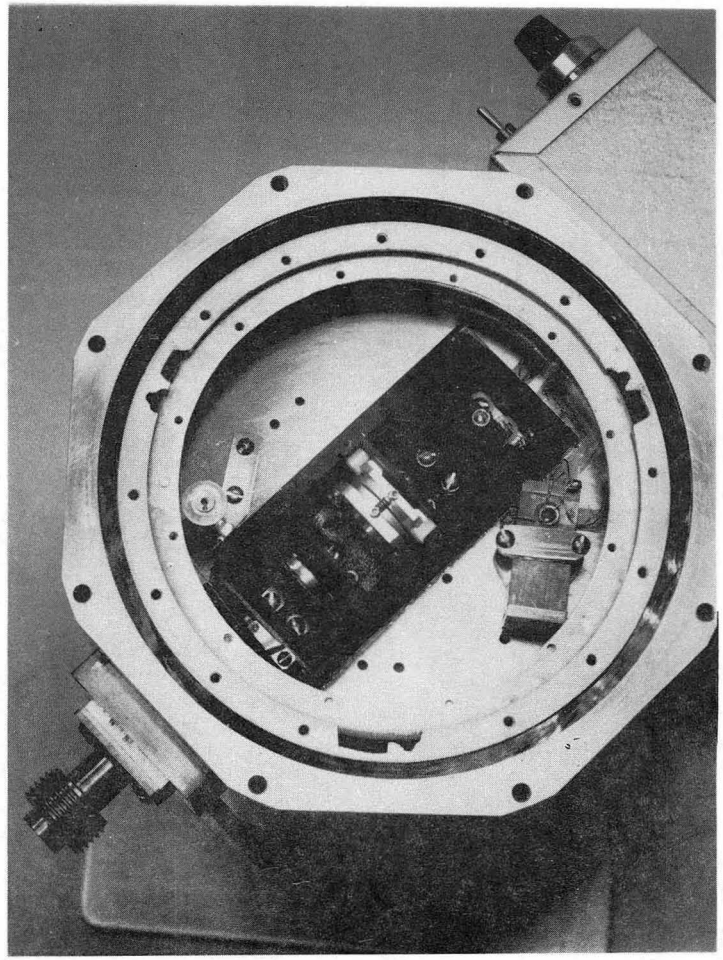

CBB 817-6974

Fig. 4. View of liquid He temperature working space showing filters, detector, and JFET housing.

The photon signal incident upon the detector is produced externally and cold-filtered within the dewar. An external chopper switches the IR source between 77 and 300 K blackbodies. The aperture in the light pipe alternately sees the reflected light from the 77 K blackbody (a black cone immersed in liquid nitrogen) and the room temperature radiation from the back wall of the chopper box. Inside the dewar, a rotating wheel with a mechanical connection to the outside allows an internal aperture (ϕ = 1 mm) to be opened and closed externally.

The low background condition for detector testing is achieved with a combination of reduced filter transmission and the geometric factor imposed by the size of the apertures. Appendix 1 contains a sample signal calculation and also a diffraction analysis of the relevant geometry. Diffraction effects must be considered because of the long wavelengths and small apertures involved. When the internal aperture is open, the light which reaches the detector is internally filtered by means of narrow band filter trains consisting of Fabry-Perot filters and reststrahlen salt filters[7]. The filters were fabricated and characterized in Professor Charles Townes' group by Dan Watson of the Physics Department, U.C. Berkeley[8]. Table 1 contains the descriptions and measured transmission for filters which were used for testing at λ = 93 and 42 μm. These filters were designed so that λ_{peak} coincides approximately with the peak of the spectral response of Ge:Ga and Ge:Be respectively. The filters are independently mounted along the optical axis on sliding baffles and are heat sunk directly to the copper plate by two screws and pure indium foil.

TABLE 1.

Filter Characteristics

λ Peak (μm)	Filter Components	Transmission (%)	Bandwidth ($\pi/2\Delta\lambda$FWHM)	Q
42.8	42 μm Fabry-Perot .7 mm LiF .5 mm KBr 2 monolayers 5-10 μm diamond dust	13.0	.79 μm	85
93.2	93 μm Fabry-Perot .5 mm KCl 1.0 mm BaF_2 2 mil black polyethylene 1 monolayer 6-12 μm diamond dust 7 mg ZnO	27.0	1.05 μm	140

The detector is located inside its integrating cavity at the far end of the box. The temperature of the detector and its surroundings is monitored by a 1 kΩ Allen-Bradley carbon composite resistor. The resistor is enclosed in a small copper block and heat sunk to the copper plate. Special care was taken to make the box light tight. A double cover with a meandering pump-out groove was used, and all surfaces within the box are covered with 3M flat black paint. With the shutter aperture closed, the detector should see no other radiation than the 4 K blackbody radiation of its surroundings. At the wavelengths of interest here, this photon flux is negligible:

($< 2 \times 10^{-19}$ photons/sec/μm at 42 μm).

That the precautions taken are effective in preventing measurable light leaks is indicated by the very high detector impedances ($10^{10} - 10^{12}\,\Omega$) that are routinely measured for most detectors under dark conditions.

The photoconductor signal is amplified by a standard transimpedance amplifier[9] (Fig. 5). The input stage consists of two matched junction FETs (J230 selected by Infrared Laboratories). The JFETs are located inside a light-tight copper housing with glass feed-throughs which are opaque to far IR radiation. They are mounted off the He temperature plate on a thin wall fiberglass tube. A 1.0 KΩ Allen-Bradley resistor is glued with epoxy resin to the JFETs. A constant voltage applied across the resistor together with the power dissipated by the JFETs keeps the operating temperature at approximately 77 K.

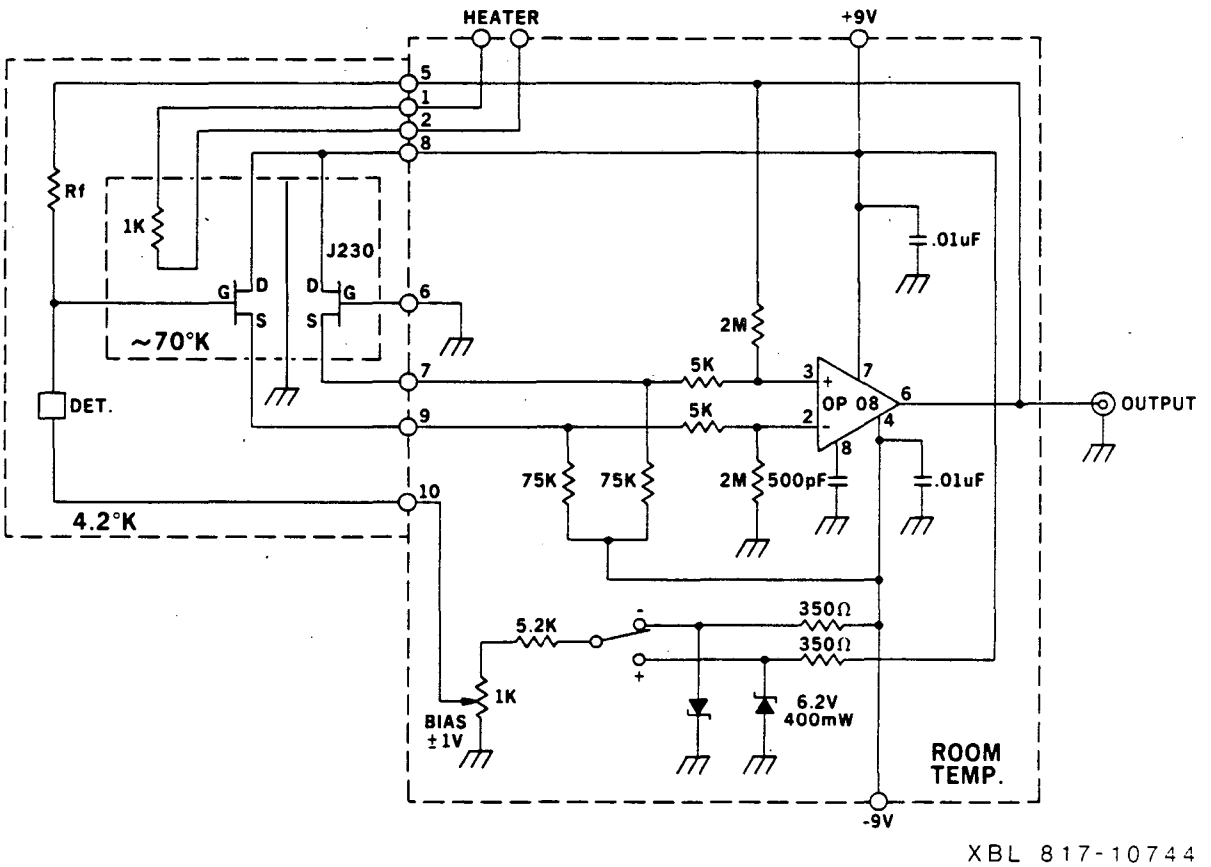

Fig. 5. Transimpedance amplifier schematic.

The feedback resistor connecting the output to the gate is an Eltec Model 102 resistor with a room temperature resistance of $10^{10}\ \Omega$. Table 2 gives measured resistance values for temperatures from 2.5 - 4.2 K. The voltage drop measured across the feedback resistor (i.e., the output voltage) is divided by the feedback resistance to obtain the value of the current flow through the detector under a fixed bias. The output signal from the transimpedance amplifier is fed directly into a lock-in amplifier for rms values of a chopped signal at any frequency. Noise measurements (taken under DC illumination) are obtained with the aid of a Hewlett-Packard Model 3582A Fast Fourier Transform spectrum analyzer.

TABLE 2.

Temperature (K)	$R_{Feedback}$ (Ω)
4.2	2.35×10^{10}
3.8	2.40×10^{10}
3.3	2.50×10^{10}
3.0	2.60×10^{10}
2.5	2.75×10^{10}
2.3	2.85×10^{10}

2.2 Detector Evaluation Procedures

Complete evaluation of the performance of a photoconductor requires extensive measurements as a function of several variables. Temperature, background flux, applied bias, and chopping frequency are all experimental variables for detector operation. Our method of signal

generation allowed for little variation in background flux. The temperatures of the external blackbodies, the filter transmissions, and the aperture sizes were fixed, uniquely determining the flux levels. The measurements to be described, therefore, are primarily measurements of signal (responsivity) and signal-to-noise (NEP) as a function of bias, chopping frequency, and detector temperature.

Detectors were produced from 1 mm slices of Czochralski-grown Ge crystals. Boron implanted contacts (1×10^{14} cm^{-2}, 25 keV and 2×10^{14} cm^{-2}, 50 keV) were used to provide ohmic tunneling contacts at low temperatures[10]. Layers of titanium (~ 550 Å) and gold (~ 8500 Å) were deposited by Ar sputtering to provide areas for electrical contacts as well as mechanical mounting. After metallization, the detectors were heated to 300°C for ~ 1 hour in Ar gas to anneal damage from the implantation, activate the B dopant (i.e., allow the boron impurities to find substitutional lattice positions), and relieve stress in the metal layers. The bare detector surfaces were polish etched in a 4:1 mixture of HNO_3:HF, rinsed with electronic grade methanol, and dried with boil-off N_2. Detectors were soldered with pure In to a 1 mm diameter carbon steel mount. Final detector size was 1 x 1 x 3 mm with 1 mm between the contacts. The detectors were mounted inside an integrating cavity (Fig. 6) with a 1 mm aperture.

In view of the exponential dependence of carrier freeze out in semiconductors at low temperatures, a change of even .5 K in detector operating temperature can have a major effect on detector performance. In the dewar, the integrating cavities are heat sunk directly to the bottom plate of the liquid-helium-containing vessel, and detector temperatures of 1.2 - 4.2 K can be attained by varying the pressure

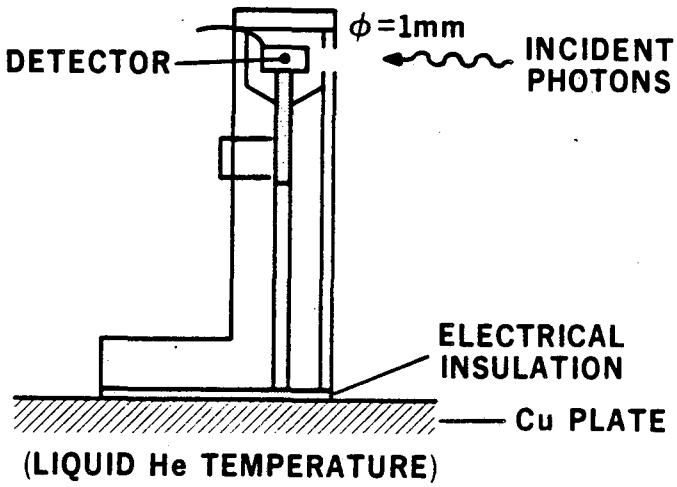

Fig. 6. Detector integrating cavity.

above the liquid. Detectors at temperatures from 2 - 4.2 K were studied in this manner. Lower temperatures are generally well beyond the range of optimum detector performance parameters. To operate at temperatures above 4.2 K, the detector is "stood off" somewhat by adding additional thermal insulation (e.g., very thin teflon) between the detector cavity and the copper mounting plate. An Allen-Bradley resistor buried within the cavity body can be used to provide both heating and temperature monitoring. Special care must be taken to assure that the optical alignment is preserved for accurate responsivity measurements and that the radiation from the heater resistor is shielded.

The external chopper had a frequency range of 5 - 100 Hz. Low frequency chopping is generally used in photoconductor evaluation because the devices are used under low frequency or even DC conditions. The long lifetime required for high responsivity and sensitivity in low-background detectors leads necessarily to slow response

times. Fast response would require the incorporation of many compensating impurities to allow for fast recombination. The measured AC signal is the rms value of the modulated output corresponding to the modulated input of signal and background. Under our testing conditions, with a 300 K blackbody signal alternating with a 77 K background, the signal was large compared to the background (see Appendix 1). This is in contrast to many cases where the input signal is just a small perturbation on a large DC background. The responsivity value, however, is a normalized quantity (A/W) and so the signal size is accounted for when making detector comparisons. Both AC and DC responsivity values can be measured as a function of applied bias. The DC responsivity is simply the magnitude of the DC output from either a constant 77 or 300 K blackbody. Noise measurements were made with the detector exposed to DC illumination from the 77 K background, and background limited NEP values were calculated based on this incident power.

3. Ge:Be PHOTOCONDUCTOR DEVELOPMENT

3.1 Background

Ge:Be photoconductor development was undertaken to meet the need for improved detector performance in the 30 - 50 μm wavelength range. Ge:Ga detectors are presently used in this application. As results in Section 3.5 will show, however, the responsivity and NEP of Ge:Ga detectors decrease and increase respectively as the photon energy increases beyond the peak of the spectral response at ~ 90 μm. In a substitutional site, beryllium is a double acceptor in Ge, with ionization energies of 24.9 and 58.0 meV[11]. A spectral response measurement of Be-doped material (Fig. 7) shows that the threshold wavelength is at 55 μm with a peak response at ~ 42 μm. Thus, Ge:Be is an excellent choice for an optimized detector in the 30 - 50 μm wavelength range.

Ge:Be detectors were first investigated by Shenker et al in 1967[12]. These authors reported problems with impurity banding in material with Be concentrations in excess of 1×10^{16} cm^{-3}, and a loss of electrically active Be during crystal growth in crystals with [Be] < 10^{17} cm^{-3} was also observed. More recently, Santa Barbara Research Corporation[13] (SBRC) and the European Space Agency[14] (ESA) have done developmental work on Ge:Be detectors using material produced by the zone-leveling technique. The highest detective quantum efficiency to date has been reported by ESA and is equal to 10% at a background of 3×10^{8} photons/second. Despite the encouraging early detector results, however, the difficulties associated with the growth of Ge:Be crystals, both in terms of Be doping and crystallography, have prevented these detectors from being fully developed, characterized, and utilized.

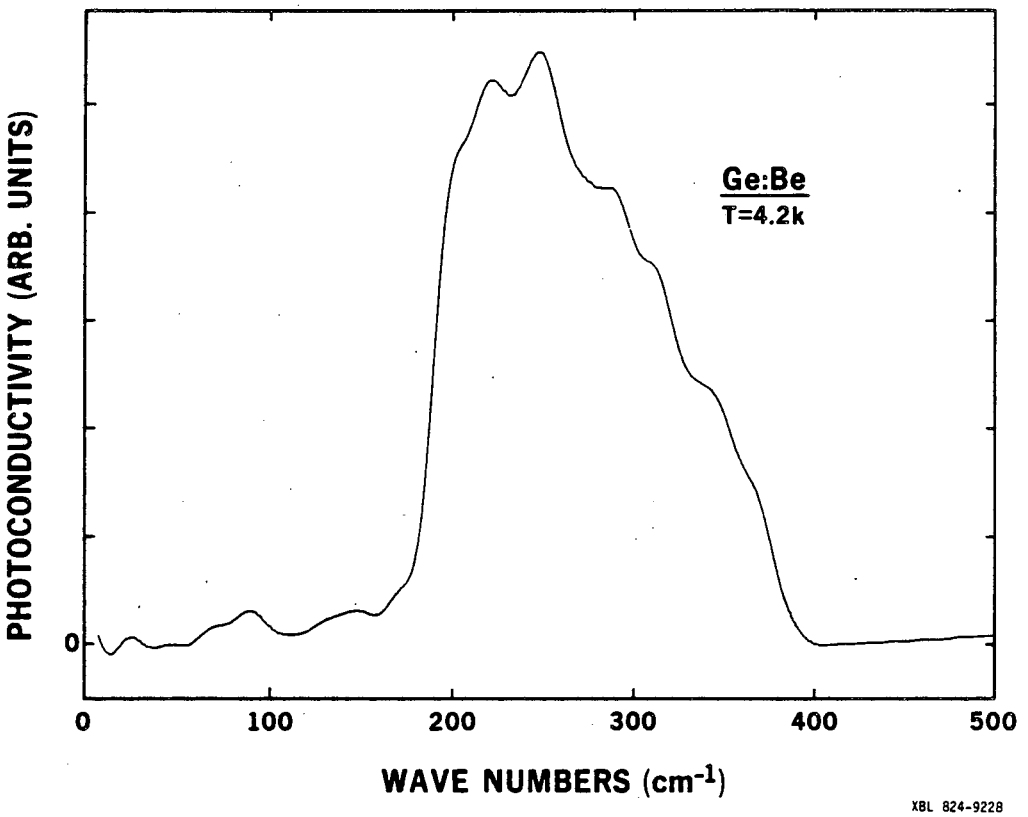

Fig. 7. Unnormalized response of Ge:Be, [Be] = 1 x 10^{15} cm^{-3}. The strong cutoff at 400 cm^{-1} is due to the effect of the beam-splitter. Near the onset and peak of the response, however, the power output is fairly constant.

3.2 Ge:Be Single Crystal Growth

In addition to the unique wavelength associated with its first ionization energy (Be is the shallowest of the deep multivalent acceptors in Ge), the high solubility of Be in the Ge lattice makes it especially suitable as a dopant for a photoconductor. Unlike the other deep double acceptors (Zn, Cd, Mn, Co, Ni, Hg), Be is as soluble in the lattice as the more commonly used Group III and Group V dopants. Shenker et al reported a maximum solubility[12] in excess of 10^{19} cm^{-3}, and Goncharov and Kervalishvili calculated a maximum solubility[15] at the crystallization temperature of ~ 4 x 10^{20} cm^{-3}. The limiting factor, therefore, in the doping of Ge:Be for photoconductor applications is

the onset of hopping conduction, and not the solubility. This is beneficial since one generally desires to have as large a concentration of dopant as possible in order to maximize the probability of photon absorption in single pass applications. The absorption coefficient α is defined by:

$$\alpha = \sigma(\lambda)N$$

where $\sigma(\lambda)$ is the photoionization cross section and N is the concentration of impurity atoms. The probability of photon absorption, of course, increases with the size of the detector. Detector size must be limited, however, for two reasons. First, the photoconductive gain is inversely proportional to the distance between the contacts. Second, exposure during space flight of the detectors to ionizing radiation must be minimized.

Because Be readily oxidizes, however, problems are encountered in crystal growth which are not present, for example, when doping with Ga. The oxygen content of the melt environment, i.e., the crucible and surrounding atmosphere, is a critical factor in determining whether Be will precipitate as stable and neutral BeO or remain as an isolated dopant which is electrically active in a substitutional site. The standard conditions for high-purity germanium Czochralski crystal growth require a silica crucible and an atmosphere of Pd-diffused H_2. Thermodynamics calculations, based on free energy of formation data and the mass action law, can give an indication of the stability of an oxide under various conditions of temperature, concentration in the melt, and environment. Calculations done following the method used by Darken[16] (Appendix 2) indicate that stable BeO would be expected to

form in equilibrium under a H_2 atmosphere when p_{H_2O}/p_{H_2} exceeds ~ 5.5 x 10^{-7} for crystal growth at 1200 K with a Be concentration in the melt of 5 x 10^{15} cm^{-3}. Since the usual ratio of H_2O/H_2 partial pressures attained during crystal growth is ~ 10^{-5}, the H_2 atmosphere used for high-purity growth is unsuitable for growing Be-doped crystals since the formation of BeO is thermodynamically favorable.

In addition, BeO is more stable, on a relative scale, than the SiO_2 which composes a silica crucible. This suggests that Be in the melt would react with a SiO_2 crucible within the limits imposed by diffusion and convection. These limits are difficult to determine since they involve complex kinetics, diffusion, and fluid flow. If a reaction did occur, however, the effect would be that the Be segregation profile would deviate from its expected form as the Be concentration in the melt was depleted by the following reaction:

$$2Be_{(m)} + SiO_2 \rightarrow 2BeO + Si$$

Thermodynamic conditions, therefore, dictate that Ge:Be be grown in a less oxygen rich environment. We have used Czochralski growth from a carbon susceptor under high vacuum (10^{-6} - 10^{-7} torr) and have avoided any significant loss of electrically active Be. Doping of the melt was achieved by using a heavily doped master alloy. The master alloy was prepared by the addition of pure Be metal to Ge. The resultant average concentration of electrically active Be was ~ 5.5 x 10^{18} cm as measured by room temperature Hall effect. Use of a master alloy provides a more controlled method of doping than the direct addition of pure Be. The weight of the dopant can be determined more precisely, and a reliable electrical measurement can be used to obtain a measure of the Be concentration to be introduced.

Four Ge:Be crystals have been grown under the conditions described (LBL crystals #703, 706, 707 and 710). All crystals were grown with a <113> orientation. Descriptions of the starting charges are given in Table 3, and Be concentration profiles for three of the crystals are presented in Fig. 8. Literature values[15] place the equilibrium segregation for Be in Ge at ~ .08. The effective segregation coefficient determined from our measured Be doping profiles is $\approx$ 0.25.

TABLE 3.

Description of the charges for Ge:Be crystals.

Crystal	Charge		
703	Ge N_D~$10^{11}cm^{-3}$ 650g	Ge:Be $5.5x10^{18}cm^{-3}$ 1.1g	
706	Ge N_D~$10^{12}cm^{-3}$ 618g	Ge:Be $5.5x10^{18}cm^{-3}$ .37g	
707	Ge N_D~$10^{11}cm^{-3}$ 720g	Ge:Be $5.5x10^{18}cm^{-3}$ .57g	Ge:Sb $7.8x10^{14}cm^{-3}$ 7.6g
710	Ge N_A-N_D $10^{11}cm^{-3}$ 747g	Ge:Be $5.5x10^{18}cm^{-3}$ .54g	Ge:P $2x10^{18}cm^{-3}$ .075g

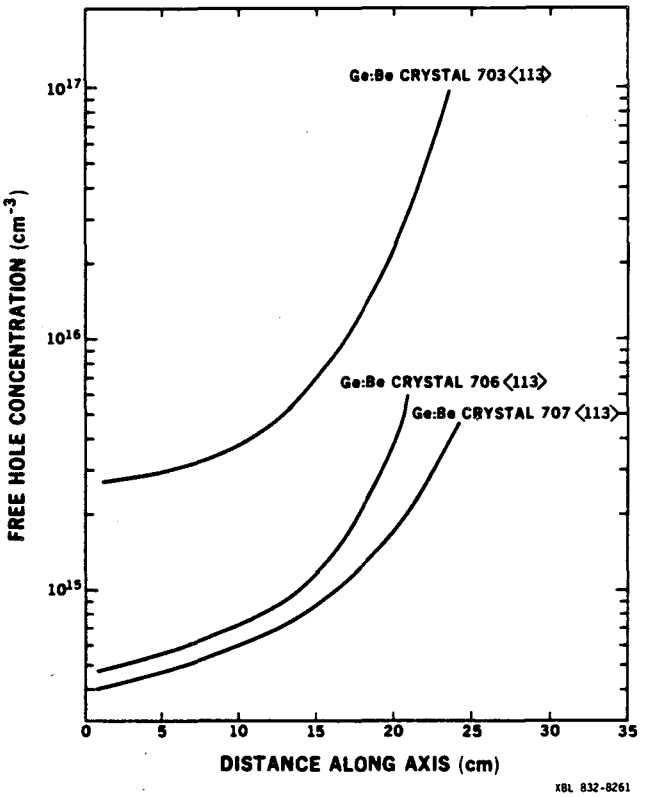

Fig. 8. Be doping profiles for Ge:Be crystals #703, 706, and 707.

3.3 Crystal Characterization and Hall Effect

Characterization of Ge:Be single crystal material prior to the evaluation of a photoconductor included measurement of Be concentration, evaluation of the crystallography, and determination of the net type and concentration of shallow impurities (i.e., ionization energies less than $E_{(Be)}$ = 24.9 meV). An estimate of the Be concentration over the entire length of the crystal was made with a simple resistivity measurement. Current is passed along the axis of the crystal, and voltage measurements are made at 1 cm intervals of the length. For the doping levels involved (10^{14} - 10^{16} cm^{-3}), this measurement was made at room temperature since the number of free carriers due to the presence of Be far exceeds the intrinsic carrier concentration due

to thermal generation at 300 K (~ 10^{13} cm^{-3}). Using the known mobility for holes in Ge at room temperature[17] and a simple calculation for the resistivity across a truncated cone, the hole concentration p is obtained [$p = (\mu e \rho)^{-1}$]. Since Be is a double acceptor and is completely ionized at room temperature, the number of holes is equal to twice the Be concentration. The Be concentration profiles in Fig. 8 were determined in this way.

The quality of the crystallography at any given section of the crystal was determined by the use of a <113> preferential etch. Because dislocations and other crystalline defects provide trapping sites and lower the mobility of free carriers in a photoconductor, single-crystal material with low dislocation density is generally required for optimum performance. An etchant of composition $HF:H_2O_2:Cu(NO_3)_2$ 2:1:1 [HF-50%, H_2O_2-30%, $Cu(NO_3)_2$-10%], used for ~ 6 min at 20°C, provided a good qualitative indication of the dislocation density. The result of a preferential etching process does not give an accurate quantitative value for the dislocation density but it does clearly indicate any polycrystalline regions or non-uniformities in the dislocation distribution across a crystal slice.

Under high-purity Ge growth conditions, low dislocation density (< 1000 cm^{-2}) is easily attained, and crystals for certain applications can also be grown dislocation free[18]. When growing under vacuum from a carbon susceptor, the control of the crystallography is more difficult. The lack of an ambient atmosphere to aid in gas convection cooling leads to very small thermal gradients at the crystal/melt interface. In addition, the Ge melt wets the carbon susceptor,

and a melt disturbance can be created when the melt pulls away from the susceptor wall toward the end of the pulling process. The result of these factors is that the dislocation density near the tails of the Ge:Be crystals is very high and small polycrystalline regions do appear in the bottom half of the crystal.

The location in the crystal of the slice needed for detector fabrication was determined by the desired dopant concentration. When a slice was taken from the head end of a crystal (the numerical suffix indicates the distance in cm from the seed end, eg. 703-4.2) the dislocation density was fairly uniform over the slice and the choice of detector material was not critical. In cases where the crystallography had deteriorated, the result of the preferential etch was observed and recorded. Detectors were only selected from single crystal, low dislocation density regions. The use of a preferential etch allows small detectors with good crystallography to be selectively prepared from any crystal slice.

When preparing Be-doped materials for photoconductor applications, the concentration of residual impurities, such as B, Al, P, etc. is also an important material parameter. As will be discussed in Section 3.4.3, shallow residual impurities have a major effect on the photoconductive response from the deeper Be level. Undoped crystals grown from a carbon susceptor are generally p-type. This is believed to be due primarily to the activation of Al which exists as electrically neutral compounds in the zone refined charge[19].

The net type and concentration of underlying shallow impurities was determined with variable temperature Hall effect. Hall effect measurements in combination with resistivity measurements yield independent

values for the free carrier concentration and mobility. Detector materials were evaluated in this manner over a temperature range of 300 K to approximately 6 K. The van der Pauw geometry[20] was used with samples measuring 7 x 7 x 1 mm^3 (Fig. 9). Either B^+ implanted contacts or Ge-In alloyed contacts were made at each of the four corners.

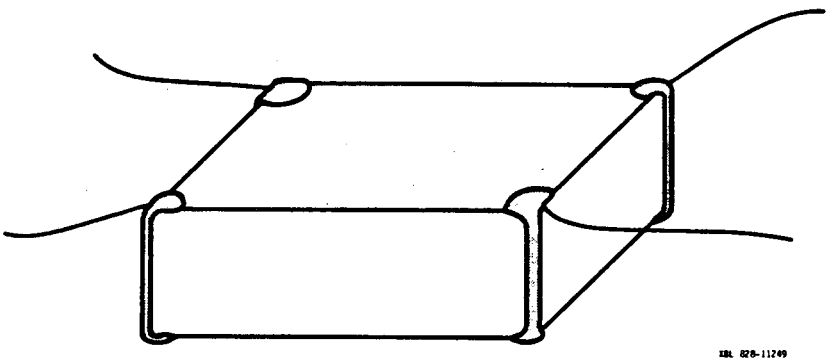

Fig. 9. Application of contacts to van der Pauw geometry samples.

The type and concentration of the net shallow impurities can be determined by the shape of an Arrhenius plot of ln (free carrier concentration) versus T^{-1}. Figure 10 illustrates schematically the nature of the "freeze-out" for material with $N_{A(shallow)} > N_{D(shallow)}$ and $N_{D(shallow)} > N_{A(shallow)}$ respectively. In both cases, the initial decrease in extrinsic carriers occurs due to the freeze-out of the second ionization stage of the Be, Be^{--}. This is followed by freeze-out of the first ionization stage, Be^{-}. In the first case, the shallow slope at low temperatures is due to the freeze-out of the uncompensated shallow p-type impurities. The net acceptor concentration is determined by estimating the point at which the shallow freeze-out begins. In the

second case, the slope of the freeze-out curve is determined only by the ionization energy of the Be level. The shallow acceptors do not appear since they are fully compensated. The degree of compensation of the Be level is indicated by the point at which the slope changes from $E_{Be}/2K$ to E_{Be}/K.

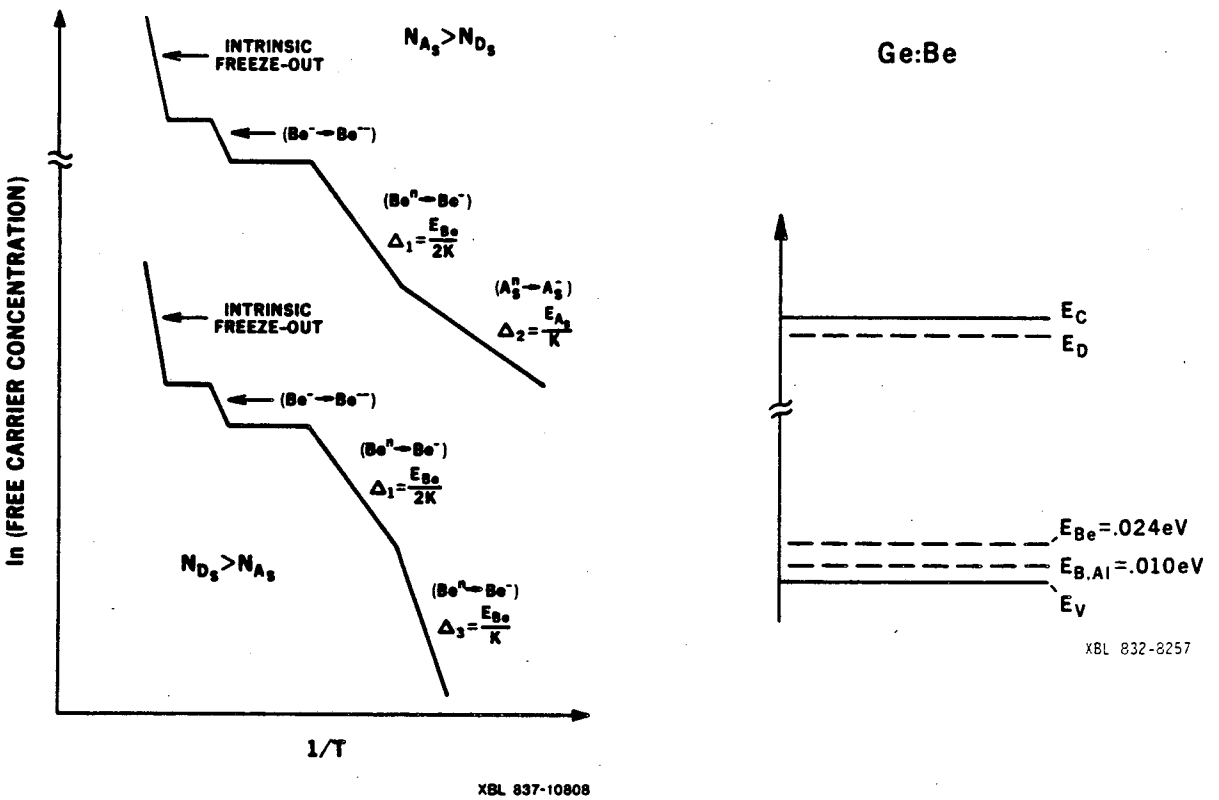

Fig. 10. Schematic Hall effect results for Ge:Be with: 1) N_A(shallow) > N_D(shallow) and 2) N_D(shallow) > N_A(shallow).

The Hall effect results for the four Ge:Be crystals are presented in Figs. 11 - 14. The scattering factor, r, was assumed to be one, as in the high field limit. Since the purpose of the Hall effect analysis was simply to determine the type and approximate net concentration of shallow impurities, no attempt was made to fit the data with a model based on the appropriate multiple levels and degeneracy factors, though

this type of analysis can be done[21]. The results show that crystals #703, 706, and 707 had a net excess of shallow acceptors, while #710 had a net excess of shallow donors. With the exception of crystal #707, all the results correspond to the doping levels predicted from the weight and doping concentration of the crystal charge. In the case of #707, the high net concentration of shallow p-type impurities is unexplained, especially in view of the addition of an n-type master alloy. Accidental contamination of the charge or of the crystal growth environment is a plausible explanation when one considers the magnitude of the effect in question (i.e., $10^{13}/10^{22} < 1$ ppb).

3.4 Ge:Be Photoconductor Evaluation

The performance of five Ge:Be photoconductors was characterized for both AC and DC response. Table 4 identifies the detectors and gives the associated material parameters that were determined from resistivity and Hall effect measurements. The behavior of the detectors was studied primarily as a function of applied bias voltage and operating temperature. Behavior as a function of applied field reveals information about the nature of breakdown phenomena in the device, indicates the impedance of the material, and establishes an optimum operating point for a detector under a given flux and at a given temperature. The temperature dependence of device performance provides information on carrier trapping and lifetime and also allows one to observe effects which are associated with the freeze-out of thermal carriers. Chopping frequency was not a major variable in this work, and all AC detector results reported are for 20 Hz unless otherwise

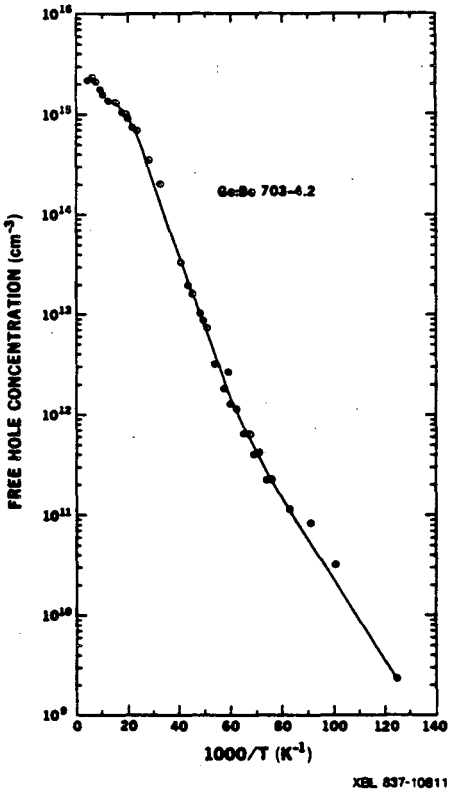

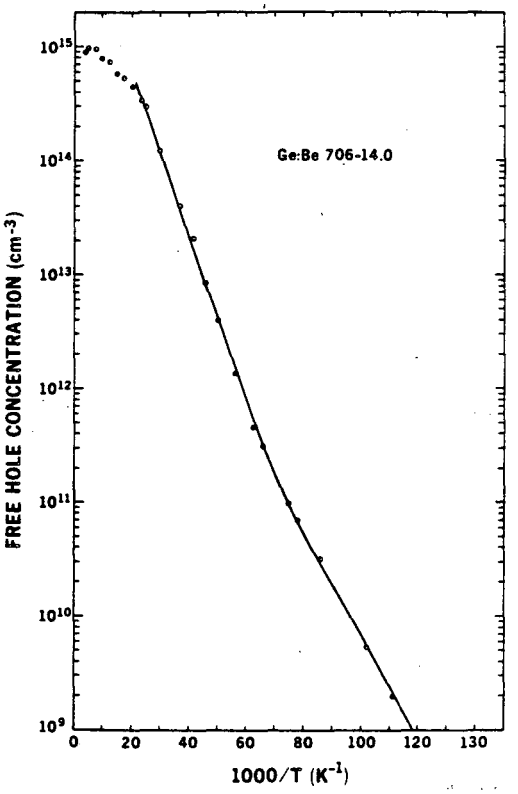

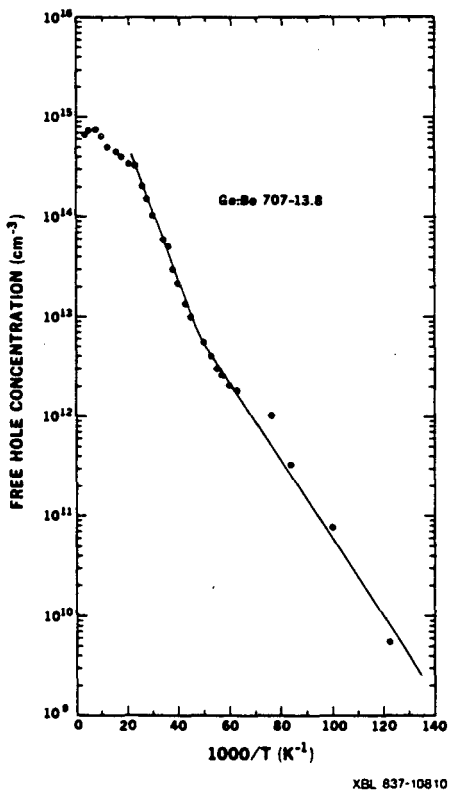

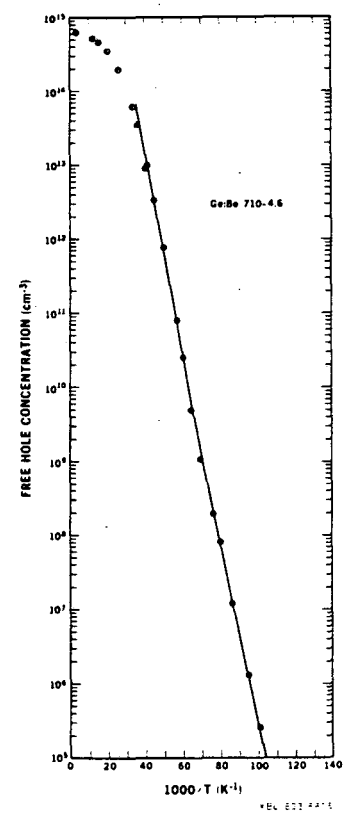

Figs. 11 - 14. Carrier freeze-out as a function of inverse temperature for Ge:Be detector materials.

noted. The background flux at 42 μm was 1.5×10^8 p/s (7.13×10^{-13} W) with a chopped signal of 7.4×10^8 p/s (3.4×10^{-12} W peak to peak).

Ge:Be detector results will be discussed in terms of three variables: Be concentration, degree of compensation, and operating temperature.

TABLE 4. Material Parameters for Ge:Be Photoconductors

Detector	Be Conc. (cm^{-3})	Shallow Majority Levels	Net Concentration of Shallow Levels (cm^{-3})	Estimated N_D (cm^{-3})
703- 4.2	1.3×10^{15}	acceptors	8×10^{11}	$\sim 10^{11}$
706-14.3	5.0×10^{14}	acceptors	5×10^{11}	$\sim 10^{12}$
707-13.5	3.5×10^{14}	acceptors	7×10^{12}	$\sim 10^{13}$
710- 9.5	5.0×10^{14}	donors	6×10^{13}	

3.4.1 Be Concentration. One of the parameters that must be optimized in the development of a photoconductor material is the dopant concentration. In some cases, the upper limit of concentration is imposed by the solubility of the dopant in the lattice. For Ge:Be, however, as well as for most Group III and V impurities in Ge and Si, a more stringent upper limit is imposed by the onset of either hopping or banding conduction. These effects occur when the dopant concentration becomes high enough that carriers can either "hop" (or tunnel) from one site to a neighboring site which is ionized due to compensation, or, at even higher concentrations can begin to move freely in a band of overlapping excited state wave functions. Hopping and banding are detrimental to photoconductor performance because they decrease the impedance of the detector material and provide substantial current flow and current noise even in the absence of photon-generated carriers.

As previously mentioned, the limit to lower concentration is generally imposed by the need for a maximum absorption coefficient. In addition, the primary dopant concentration is often a dominant factor in determining carrier mobility in cases where compensation is low and neutral impurity scattering at low temperatures is significant. The mobility affects not only the magnitude of the output signal, but also the maximum bias which can be applied prior to the "breakdown" of the device. Breakdown in photoconductors occurs by the mechanism of impact ionization. When free carriers acquire sufficient energy from the applied field, they can impact ionize other neutral impurities. As this effect multiplies, there is a large increase in current flow through the detector, the impedance drops rapidly, and a photon-generated signal can no longer be produced. The velocity which a free carrier acquires in a given field is determined by its mobility and lifetime, and so a decrease in dopant concentration will result in an earlier breakdown in cases where neutral scattering is significant. Optimum dopant concentration, therefore, is a compromise between the need for maximum absorption, maximum signal, and minimum noise.

SBRC had established with low temperature resistivity measurements that hopping conduction was a factor in Be-doped detectors with a Be concentration[13] in excess of ~ 2×10^{15} cm^{-3}. Based on this result, concentrations in the range of 3.5×10^{14} cm^{-3} to 2.3×10^{15} cm^{-3} were investigated. In Fig. 15, responsivity and NEP values as a function of bias at 3.8 K are presented for the four detectors which had net shallow acceptor concentrations. A number of conclusions can be drawn from this comparison.

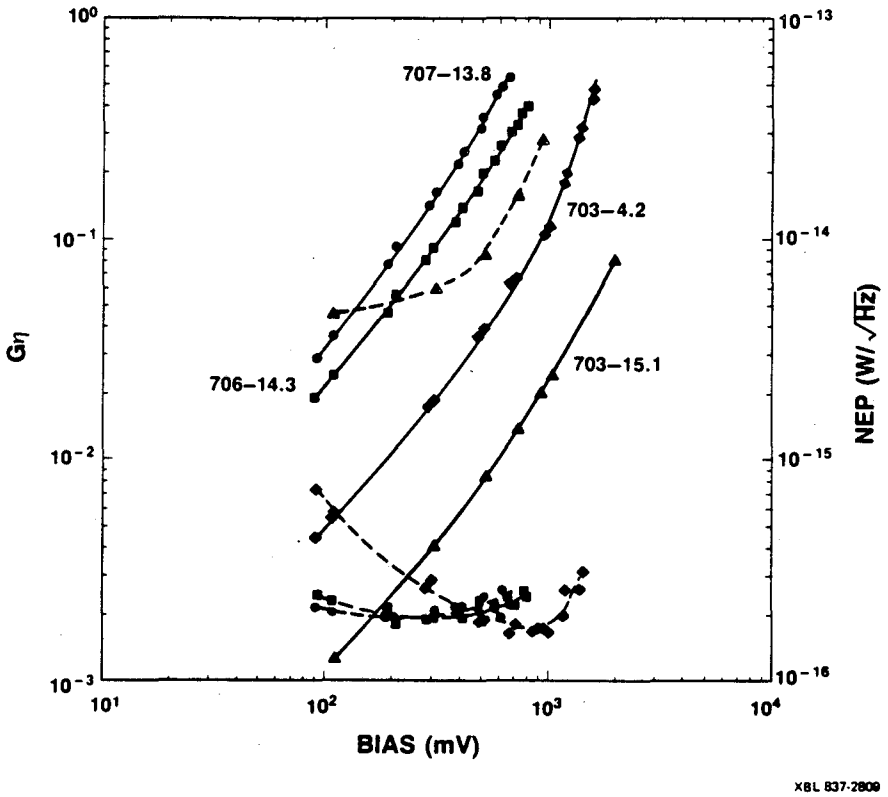

Fig. 15. Responsivity and NEP as a function of bias. T = 3.8 K, chopping frequency = 20 Hz. Solid lines indicate responsivity. Dashed lines indicate NEP. $NEP_{back.lim.}$ =1.15 x 10^{-16} W/ $\sqrt{Hz}$.

The data presented were generally taken in the optimum bias range for these detectors. Three bias regimes can usually be identified for a photoconductor. At very low bias (< 100 meV for Ge:Be), detector performance is referred to as amplifier limited, indicating that the noise associated with the amplifier circuit (including the Johnson noise of the feedback resistor) is larger than or comparable to the photon noise. For the circuit shown in Fig. 5, the amplifier noise is ~ 2 x 10^{-6} V/$\sqrt{Hz}$ at 4.2 K. In addition, noise associated with thermal generation and recombination can also be a factor at low bias. The result is a high NEP at low bias. As the bias is increased, both the

signal and noise increase. The contribution of the amplifier noise becomes small compared to the increasing current noise associated with photoionization. The minimum NEP is usually achieved within this region. As the bias is increased toward the breakdown point, the noise increases much faster than the signal, and the NEP rises rapidly as impact ionization begins.

In Fig. 15, one observes that the responsivity increases with decreasing Be concentration. This trend can be explained qualitatively to first order by the increase in mobility that is caused by decreased neutral scattering due to the decreased number of Be atoms. This simple interpretation, however, is complicated by the effect of charged impurity scattering from the compensated shallow donors and acceptors. Although the concentration of these centers is much lower than the concentration of Be (10^{11} - 10^{12} cm^{-3} compared to 10^{14} - 10^{15} cm^{-3} Be), the individual magnitude of the scattering effect of a charged scattering center is greater than a neutral center because of the presence of the Coulomb potential.

The number of ionized scattering sites in a p-type crystal with N_D compensating impurities is $n = 2N_D + Q$ where $Q \cong$ the number of photon-generated ionized sites. Q can be neglected in low background cases, and so the number of ionized scattering sites is simply two times the number of donors in the material. Equilibrium Hall effect and resistivity measurements on Ge:Be can only indicate the net shallow acceptor concentration, $N_A - N_D$, when the material is underlying p-type. The values given in Table 4 for N_D in these cases, therefore, are only order-of-magnitude estimates based on experience

with residual impurity levels obtained in high-purity Ge for various growth conditions. Based on these estimates, one would expect the largest contribution from charged impurity scattering to occur in detector 707-13.8. The responsivity at this lower Be concentration is still increased, however, in comparison to detector 706-14.3. One can conclude that neutral scattering, although it may or may not be dominant in these detectors, is significant in determining the mobility even when the concentration of charged impurities exceeds 10^{12} cm^{-3}. A complete analysis of the hole mobility in these detectors would require that absolute concentrations of both shallow acceptors and donors be obtained with photo Hall effect and that the Hall effect data be extended through the detector operating temperature range.

The Be concentration also affects the maximum bias which can be applied to the detector before the onset of breakdown. Signal and noise data were taken for these detectors up to the bias at which saturation of the op-amp occurred; as the Be concentration increased, this maximum bias also increased. This reflects again the decrease in mobility which occurs with increasing Be concentration. With a lower mobility, a higher field is necessary to accelerate the carrier to the energy at which impact ionization begins to occur (assuming a constant lifetime). The average breakdown field for the Ge:Be detectors is ~ 10 V/cm at 4.2 K. As expected, this is larger than the breakdown field for Ge:Ga (~ 3 - 4 V/cm at 4.2 K), but less than the breakdown fields reported[5] for deeper levels such as Ge:Zn (405 V/cm, [Zn] = 1×10^{16} cm^{-3}, $[N_D] < 1 \times 10^{14}$ cm^{-3}) or Ge:Cu (630 V/cm, $[Cu] = 1.8 \times 10^{16}$ cm^{-3}, $[N_D] \sim 1 \times 10^{14}$ cm^{-3}).

Turning to the NEP results, one observes that the NEP for these detectors (excluding for the moment #703-15.1) is fairly flat over a bias range of several hundred meV. The optimum bias, (defined as the bias at which minimum NEP is attained) increases slightly with increasing Be concentration. This is due to the changes in mobility and breakdown voltage which have previously been discussed.

The responsivity and NEP were presented at 3.8 K because the lowest NEP values were obtained at this temperature. The responsivity of Ge:Be detectors is highly temperature dependent; this phenomenon will be discussed in detail in a following section. One sees that NEPs $< 2 \times 10^{-16}$ W/$\sqrt{\text{Hz}}$ were attained by detectors #703-4.2, #706-14.3, and #707-13.5. The lowest experimental NEP (1.7×10^{-16} W/$\sqrt{\text{Hz}}$ for detector #703-4.2 at 10 V/cm and 3.8 K) corresponds to a detective quantum efficiency of $\eta = 46\%$. In general, one would place the optimum Be concentration in the range of $5 \times 10^{14} - 1 \times 10^{15}$ cm^{-3}. After considering the effects of compensation and operating temperature on Ge:Be detectors, it will become apparent that the optimum Be concentration could vary somewhat depending on the application and operating conditions.

The combined responsivity and NEP results for detector #703-15.1 show the effect of exceeding a certain upper bound in the primary dopant concentration of a photoconductor. The decrease in responsivity can be attributed in large part to the decreased mobility due to the increase in neutral scattering. In addition, however, #703-15.1 shows a large decrease in signal-to-noise ratio, as indicated by the order of magnitude increase in NEP. Noise results, presented in Fig. 16,

show that this is not simply a result of an extended amplifier noise limited regime, but that the noise actually increases more rapidly with bias than in the case of the less heavily doped material.

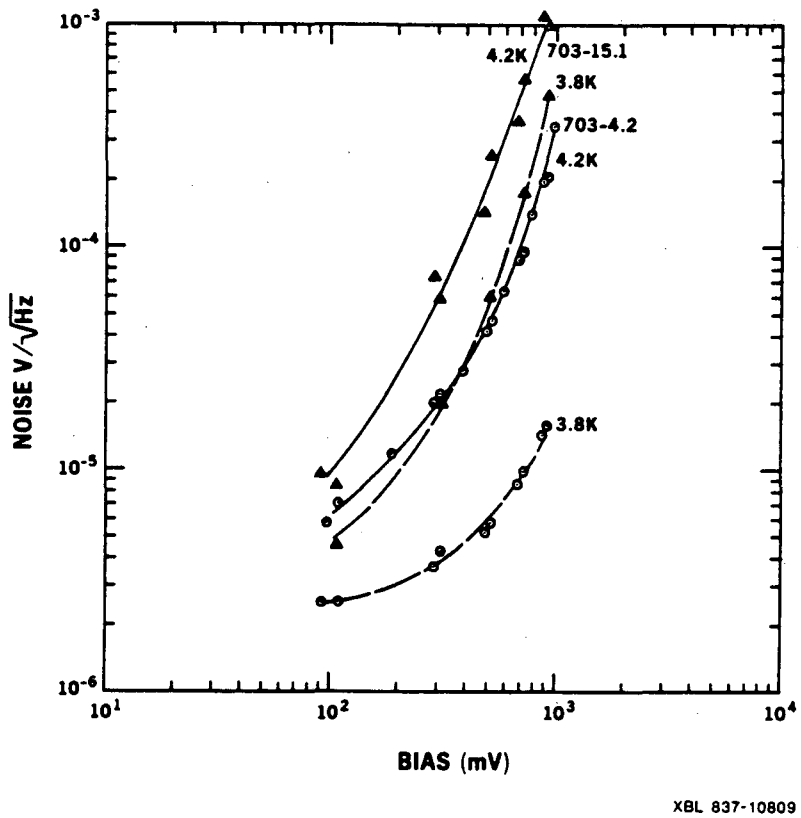

Fig. 16. Noise as a function of bias under DC background illumination. T = 3.0 K.

As previously discussed, one effect of exceeding the optimum concentration in a photoconductor is an observed decrease in the "dark impedance" of the detector due to the presence of hopping conduction. In thermal equilibrium, the free carrier concentration in a compensated extrinsic semiconductor can be approximated in the freeze-out regime by:

$$n \sim N_o \, e^{-E_i/kT}$$

where N_o is the dopant concentration. If conduction occurred solely as a result of thermally generated holes, one would expect an exponential decrease in current with decreasing temperature, modified by the temperature-dependence of the lifetime and the mobility. Neutral impurity scattering has been shown to be a significant factor in determining the mobility in the detector at these Be concentrations and temperatures. Since neutral impurity scattering is only weakly temperature-dependent[22], the change in dark current with temperature should approximate the change in the number of free carriers modified by the lifetime effect.

In Fig. 17, the thermal current is plotted as a function of inverse temperature for detectors #707-13.5, 703-4.2, and 703-15.1 at a constant bias. In Fig. 18, the temperature dependence of the lifetime has been removed by considering the temperature dependence of the responsivity of these detectors at the same bias (see temperature dependence section 3.4.3 and Figure 24). In effect then, Fig. 18 shows an "effective number" of carriers as a function of temperature. As indicated, the slope of the curves for detectors 703-4.2 and 707-13.5 corresponds to an ionization energy of approximately 10 meV, the ionization energy of shallow acceptors in Ge. One sees, however, that there is a conduction mechanism in the more heavily doped material that allows it to carry current independent of the availability of thermally generated free carriers. The actual number of thermally generated free carriers must decrease exponentially in all cases; the leveling off of the "effective carrier" concentration, therefore, must be due to hopping or banding, mechanisms of conduction which do not require free carriers in the valence band.

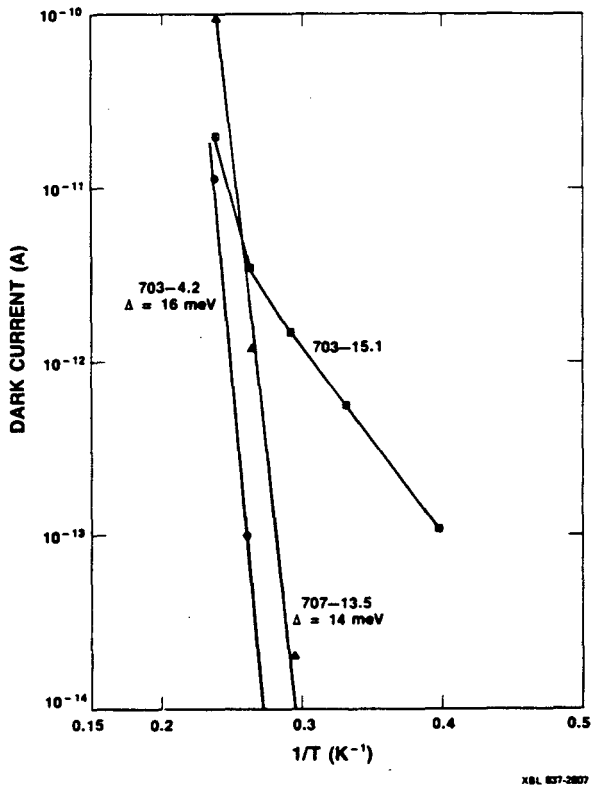

Fig. 17. Dark current as a function of inverse temperature at a constant bias field of 5 V/cm.

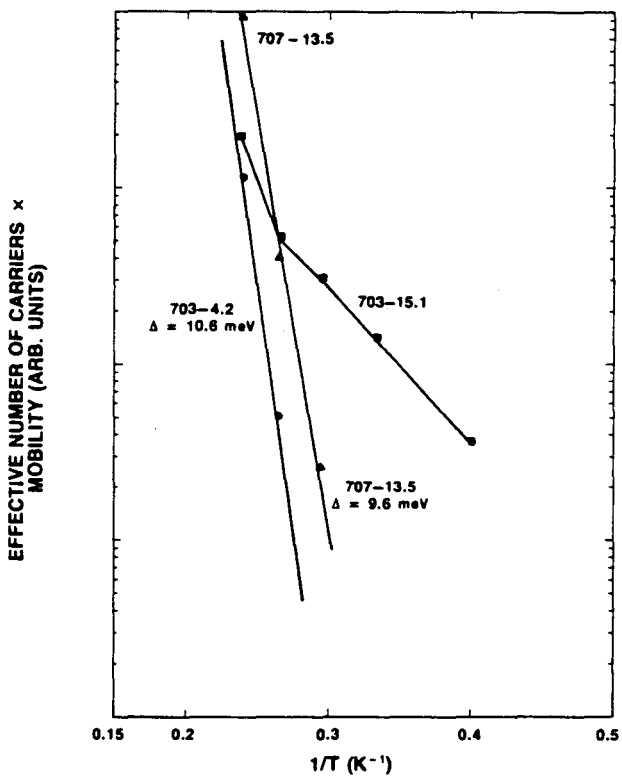

Fig. 18. Effective number of carriers x mobility as a function of inverse temperature at a constant bias field of 5 V/cm.

Data available on the phenomenon of hopping and banding in Ge indicate that the Be concentration in detector 703-15.1 is too low to cause conduction through banding[23], and so the conduction must be associated with the onset of hopping. The simple model for hopping, however, in which a free carrier (a hole in this case) moves from a neutral site to an ionized site cannot be simply invoked here because, in thermal equilibrium, there are no compensated Be atoms since the material has a net concentration of shallow acceptors. In cases where hopping has been studied in n-type materials, the presence of a D^- center (an extra electron bound to a neutral donor site) has been invoked to explain certain regimes in the $\rho(T)$ (resistivity as a function of temperature) curve[24]. Possibly an analogous model with the formation of an A^+ center could be applied in this case to explain the motion of carriers among the Be sites without the aid of compensation. The A^+ center has been observed with photothermal ionization spectroscopy (PTIS) in several shallow acceptors[25], and PTIS studies on the detector materials used in this study have confirmed its existence in Ge:Be[26].

3.4.2 Compensation. Compensation in a p-type material is generally defined as N_D/N_A, where N_A is the total number of acceptors. When discussing the effect of compensation in a multi-level Be:Ge detector, however, it is helpful to define a compensation K_s of shallow acceptors and an effective compensation K_{Be} of beryllium acceptors. In terms of concentrations:

$$K_s = \frac{N_D(\text{shallow})}{N_A(\text{shallow})} : N_A(\text{shallow}) > N_D(\text{shallow})$$

and $$K_{Be} = \frac{N_D(\text{shallow}) - N_A(\text{shallow})}{N_{Be}} : N_D(\text{shallow}) > N_A(\text{shallow})$$

When the number of shallow donors exceeds the number of shallow acceptors, the shallow acceptors are completely compensated (consider thermal equilibrium, T = 0K) and one can speak of the remaining effective compensation of the Be level. When the number of shallow acceptors exceeds the number of shallow donors, one can refer to a K_s between 0 and 1, and $K_{Be} = 0$.

In Fig. 19, the responsivity and NEP as a function of bias are presented for detectors 706-14.3 and 710-9.5. These detectors had the same Be concentration (5×10^{14} cm^{-3}), but differed substantially in the ratio of N_D(shallow) to N_A(shallow). In 706-14.3, K_s would be estimated, based on the characterization of the crystal charge, to be > 0.2 with $K_{Be} = 0$. In 710-9.5, $K_{Be} \simeq 0.1$; the shallow acceptors in this case can be referred to as "over-compensated." The increase in donor concentration increases the number of charged scattering centers ($2\ N_D$), causing a decrease in both the mobility and lifetime of free carriers.

The detector behavior reflects these changes in the transport parameters. The responsivity in 710-9.5 is decreased by an order of magnitude at 3.8 K, and the breakdown field is extended to ~ 50 V/cm as compared to 0.8 V/cm in 706-14.3. Both effects are consistent with decreased mobility and free carrier lifetime. The slope of the responsivity versus bias curve for 710-9.5 does not exceed a linear voltage dependence until very close to the breakdown point. This may be due in part to a saturation of the velocity caused by the large concentration of charged scattering sites.

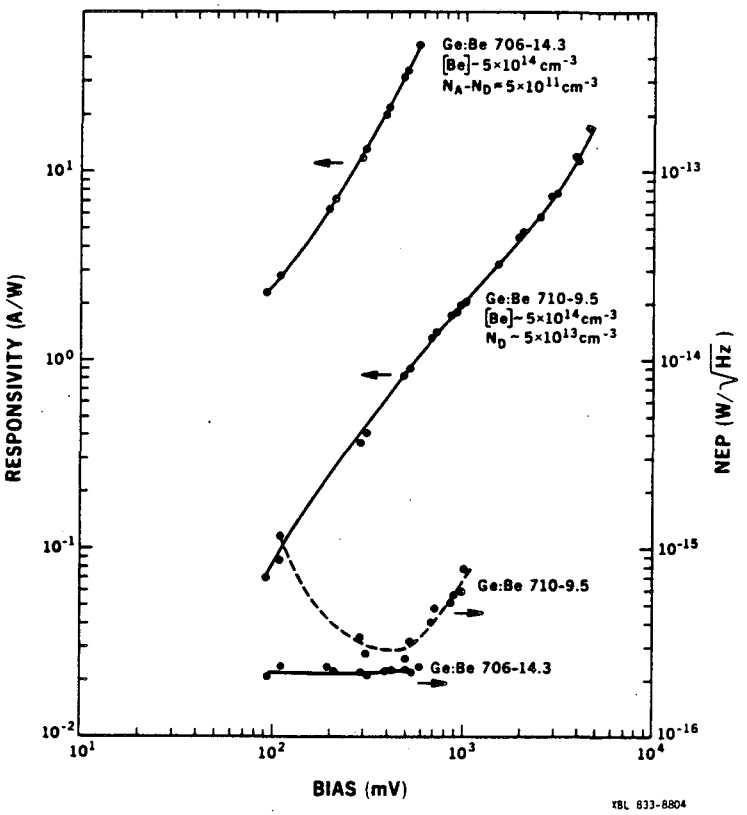

Fig. 19. Responsivity and NEP as a function of bias. T = 3.8 K, chopping frequency = 20 Hz. $NEP_{back.lim.}$ = 1.15 x 10^{-16} W/ $\sqrt{Hz}$.

The major features of the NEP versus bias curve can also be explained qualitatively. Because the signal at low bias is smaller, as is the associated photon noise current, the contribution of amplifier noise is significant, and an amplifier noise limited region is observed from 100 - 400 meV. This is not present in detector 706-14.3 because the amplifier noise is small compared to the noise of the photon-induced signal. As the signal size increases in detector 710-9.5, the contribution from amplifier noise bcomes less dominant, and the NEP approaches the minimum attained by all the Ge:Be detectors. A rise in the NEP at voltages near breakdown is characteristic of all detectors.

In this case, however, the steep degradation of the NEP at biases low compared to the breakdown bias is not understood. The symmetry of the phenomena in both the positive and negative bias modes makes a contact problem seem unlikely.

One benefit of overcompensation of shallow acceptors is the elimination of any significant thermal currents at detector operating temperatures up to 4.2 K. Measurement of this dark current over a temperature range of 2.5 to 4.5 K indicates that the impedance of the detector is greater than $10^{11}\Omega$. The high impedance of the crystal #710 material is easily understood by reference to the Hall effect result of Fig. 14. A higher impedance detector can offer better performance because it can be operated at higher temperatures to take advantage of higher responsivities without a substantial increased noise contribution from thermal generation and recombination, (i.e. no increase in NEP). In the case of detector 710-9.5, the lifetime and mobility effects of the extreme overcompensation, however, overshadow any potential benefit. The results for detector 710-9.5 indicate, however, that the expected increase in responsivity with a constant NEP does occur from 2.5 to 4.4 K. This could be utilized in the operation of an optimized detector produced from material with $N_{A(shallow)} \approx N_{D(shallow)}$, with the concentration of these impurities kept to a minimum.

A final comparison between the behavior of these two detectors clearly illustrates that the key to providing reliable Ge:Be detector material lies in the control of the shallow residual impurity concentrations. Figure 20 presents the responsivity of detectors 706-14.3

and 710-9.5 as a function of temperature. The temperature-dependence of the responsivity in detector 710-9.5 is comparable to that observed in Ge:Ga detectors. This is understood in terms of the increase in lifetime due to the decreased trapping effectiveness of excited states at higher temperatures[27]. A different phenomena is clearly at work in detector 706-14.3. In order to understand the different results in these two detectors, one must consider the temperature dependence of trapping and recombination in a multi-level system such as Ge:Be in the presence of a photon flux.

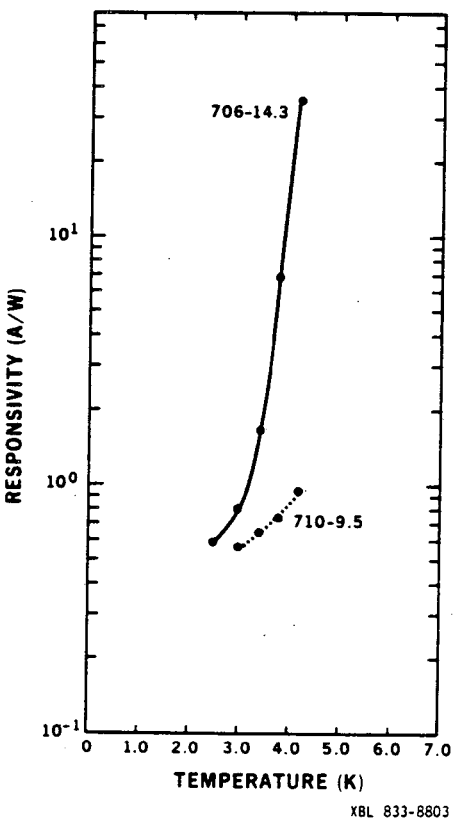

Fig. 20. Responsivity as a function of temperature. Chopping frequency = 20 Hz. Bias field = 5 v/cm.

3.4.3 Temperature. The strong temperature dependence of the responsivity exhibited by detector 706-14.3 is a unique feature of multilevel systems in which residual shallow acceptors and donors affect the photoconductive behavior in a device which is heavily doped with a semi-deep impurity. This behavior was first observed in Si:In photoconductors[28]. Indium is a semi-deep single acceptor in Si ($E_{ionization}$ = .16 eV), and this material is used as a detector in the 3 - 5 μm range, the so-called "atmospheric window". Schematic band diagrams for Si:In and Ge:Be are presented in Fig. 21. Except for the presence of a second ionization stage in Ge:Be (which plays no role when there is neither sufficient thermal nor photon energy to remove the second hole), the systems are exactly analogous. Mathematical models have recently been developed which explain the temperature dependence of the responsivity in closely compensated extrinsic detectors[29,30], and the theoretical fit to the experimental data for Si:In has been quite good. These models would predict similar behavior in Ge:Be, with appropriately scaled temperatures to reflect the smaller binding energies of shallow impurities in Ge. The results presented here are the first reported experimental confirmation for these predictions in Ge:Be.

The model proposed by Alexander et al[29] is based on the calculation of the generation-recombination equilibrium in a space-charge neutral detector under a constant background flux Q. The governing equations, adapted for Ge:Be, are presented in Appendix 3. A qualitative discussion of the behavior will be presented here.

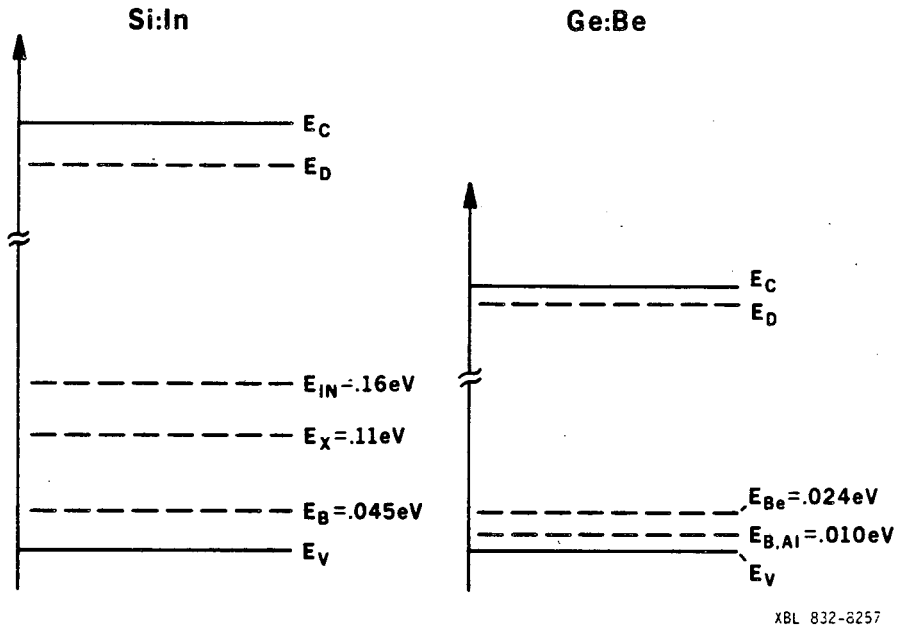

Fig. 21. Schematic band diagrams for Si:In and Ge:Be.

Figure 22 presents Alexander et al's results for dp/dQ as a function of temperature for the three Si:In cases indicated. It will be helpful to refer to this figure and to discuss this behavior in terms of various regimes of temperature and compensation. The fundamental physical principle involved is that the lifetime of free carriers in Ge:Be or Si:In is strongly affected by the thermal ionization of shallow acceptor impurities. If one assumes uniform irradiation of a single wavelength, then the detector responsivity, in amperes/watt, is directly proportional to the mobility and the derivative of the conductance with respect to photon flux.

$$R(T) \propto \mu(T) \frac{d\,p(T)}{dQ}$$

where $\mu(T)$ = mobility; $p(T)$ = carrier concentration; and Q = background flux. The lifetime dependence of the photoconductive gain is contained

in the dp/dQ term, and it is this term that the model calculates as a function of temperature.

The three cases shown in Fig. 22 will be referred to as (A) undercompensated, (B) overcompensated, and (C) exactly compensated. The compensation of interest is the compensation of the shallow acceptors, i.e., K_s, so that these cases can also be described as $K_s < 1$, $K_s > 1$, and $K_s \simeq 1$. Consider first the lowest temperature regime, the regime in which dP/dQ is temperature independent for all three cases. At very low temperatures, thermal generation from the shallow level is negligible both in comparison to the compensation and to the photon generation rate. All the shallow acceptor sites will be neutral except for the very small number which are photoionized. This is in sharp contrast to the thermal equilibrium situation in the dark. The presence of the photon flux, which preferentially generates carriers from the Be sites, shifts the location of the compensated sites from the shallow centers to the deeper Be level. In their neutral state, these acceptors are neither trapping nor recombination centers for the free holes and do not affect the free carrier concentration. The lifetime is determined just by the compensation and there is no temperature dependence. This regime applies at low temperatures regardless of the degree of compensation of the shallow acceptors. One sees from Fig. 22 that as the donor concentration increases, the lifetime and therefore the responsivity decrease, as expected.

As the temperature is increased, one enters a second regime in which the thermal ionization of shallow acceptors is no longer negligible. The onset of this regime is generally defined as the point at which the thermal generation rate exceeds the photon

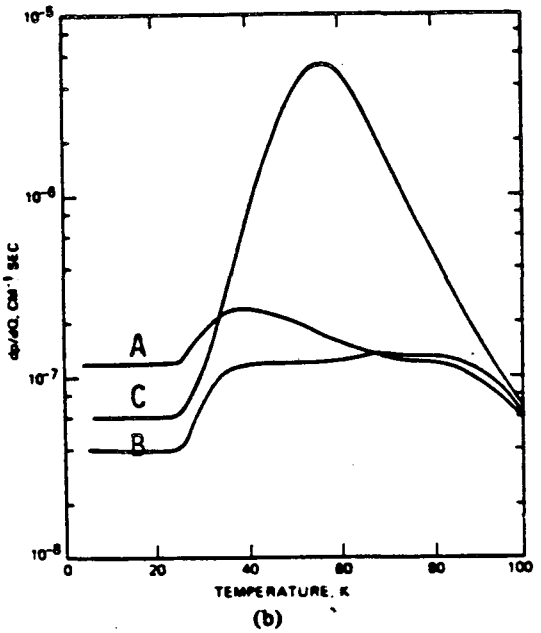

Si:In

$N_{In} = 2 \times 10^{17}$ cm^{-3}

$N_X = 5 \times 10^{14}$ cm^{-3}

Case	N_B (cm^{-3})	N_D (cm^{-3})
A	1×10^{14}	5×10^{13}
B	1×10^{14}	1.5×10^{14}
C	1×10^{14}	1×10^{14}

Fig. 22. dp/dQ as a function of temperature for Si:In cases as indicated (Ref. 29).

generation rate from the shallow level. Since the number of thermally ionized sites is an exponential function of temperature, thermal generation will quickly dominate the constant generation rate due to the photon flux. Consider first the overcompensated case, i.e., $K_s > 1$ and $0 < K_{Be} < 1$. With increasing temperature, the probability for thermal ionization from shallow acceptors increases. The additional number of ionized sites, compared to the compensation, is still very small, but the changing probability of generation causes the majority of ionized sites to shift to the shallow acceptors. The change is illustrated schematically in Fig. 23.

It is in this temperature range that the large increase in responsivity will occur. The ionized shallow acceptor sites become progressively less effective hole traps as the probability of thermal regeneration increases. Although the number of ionized sites is basically constant [$N_D >> Q$ and $> N_A$ (thermal)], the capture cross section has been reduced. The higher excited states are no longer trapping centers because the probability of escape is very high. If the temperature is increased even further, the responsivity will decrease when thermal generation from the semi-deep level becomes significant. This increases the number of ionized sites and decreases the lifetime. In addition, p_{total} becomes large with respect to $p_{photo\text{-}generated}$, and so dp/dQ becomes smaller as p increases.

All the major features of the under-compensated case can be explained by the same type of analysis (see Ref. 29). The unique case is the case in which the shallow acceptors are exactly compensated by shallow donors. In this case it is possible, in the temperature regime where the shallow acceptors are fully ionized and thermally dominated,

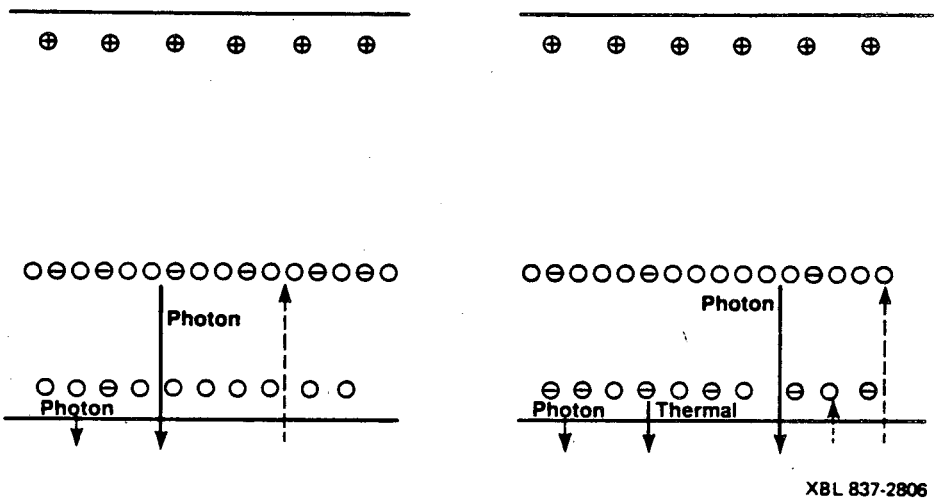

Fig. 23. Effect of increasing temperature on generation-recombination probabilities from the Be and shallow acceptor levels.

to have a very small probability of recombination into the ground state and, therefore, a very long lifetime. The effective cross section of the shallow acceptors is small and, in the case of exact compensation, there are no additional ionized Be sites (neglecting, as always, the photogenerated sites) to serve as trapping centers. Thus, a large peak in responsivity is predicted for the case of $K_s = 1$.

Figure 24 shows that this temperature dependence of the responsivity has been observed in detectors 703-42, 706-14.0, and 707-13.5. We have interpreted this behavior in terms of this model and explained the increase in responsivity primarily as an increase in lifetime due to this effect. Although mobility is also a function of temperature,

it is a weak function of temperature in comparison to the exponential increase that is observed. Initial attempts to model the Ge:Be system using the approach outlined in Appendix 3 indicate that both the temperature range over which this effect should occur (3 - 5 K in Ge) and the major features of the behavior are in good agreement with what we observe experimentally. Referring back for a moment to Figs. 17 and 18, the lifetime dependence of the conductivity was taken into account by considering the change in responsivity of the same detector under the same bias with a photon flux as solely a lifetime enhancement. In order to arrive at an "effective number" of carriers, the lifetime effect was simply factored out of the raw data.

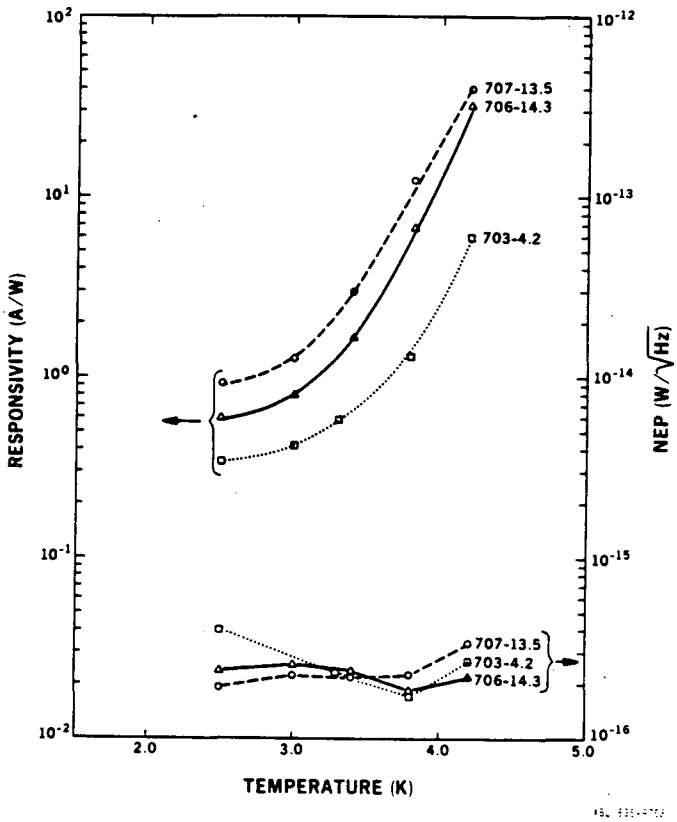

Fig. 24. Responsivity as a function of temperature at a constant bias field of 5 V/cm. Chopping frequency = 20 Hz. $NEP_{back.lim.} = 1.15 \times 10^{-16}$ W/ $\sqrt{Hz}$.

The results of Fig. 20, which compared the behavior of two detectors with similar Be concentrations but different donor concentrations, can now be understood. In detector 706-14.0, the shallow acceptors are closely compensated by the shallow donors and so the predicted temperature dependence is observed. In the case of detector 710-9.5, however, the donor concentration is so high that the majority of ionized sites are ionized Be, regardless of the temperature or the photon flux. The lifetime is always dominated by the Be ionized sites and the effect of thermal ionization of shallow acceptors is not significant. Detector 710-9.5, therefore, displays the temperature-dependent behavior that is characteristic of a standard two-level system with a lifetime fixed by the compensation.

Published results on the work performed to date by other groups developing Ge:Be detectors do not include any mention of such a strong temperature dependence of the responsivity between 4.2 and 3.0 K as has been observed with these detectors. This suggests that either the shallow residual impurity concentrations were too high in their material or the shallow levels were greatly over or under compensated for the effect to be observable.

The predicted peak responsivity for a detector in which the shallow acceptors are exactly compensated will be difficult to attain in practice. Alexander et al[29] demonstrate the extreme sensitivity of the responsivity to small shifts in compensation, and control of residual impurity concentrations to that extent is probably not feasible. In Si, neutron transmutation doping (Si → P) has been used to achieve exact compensation[28]. A similar technique could be used in Ge:Be,

although the process would be less efficient since the transmutation doping of Ge leads to the production of both donors and acceptors[31]. The compensation ratio, K, is fixed by the isotopic composition at K = 0.4.

One crystal growth scheme that might result in the exact compensation of shallow levels would be to grow a Be-doped crystal under vacuum from a silica crucible. If the starting charge had the concentration profile shown in Fig. 25, it should be possible to, in effect, superimpose the Be profile resulting in a section of the crystal having an "underlying junction." The obvious potential problem with this has been discussed previously. The Be could act to reduce the silica crucible leading to the formation of stable and electrically inactive BeO. The extent to which the kinetics of this reaction are favorable, however, is difficult to predict, and an experimental approach seems worthwhile. If the loss of electrically active Be is not in the range of orders of magnitude, the major effect may be to flatten the Be segregation profile, a not undesirable effect in the production of detector material. The extent to which the neutral BeO would affect the mobility in the detector is another unknown. If a crystal were grown in this manner, the junction could be located with variable temperature Hall effect. The mobility data obtained in this way would indicate whether there was a major effect from BeO.

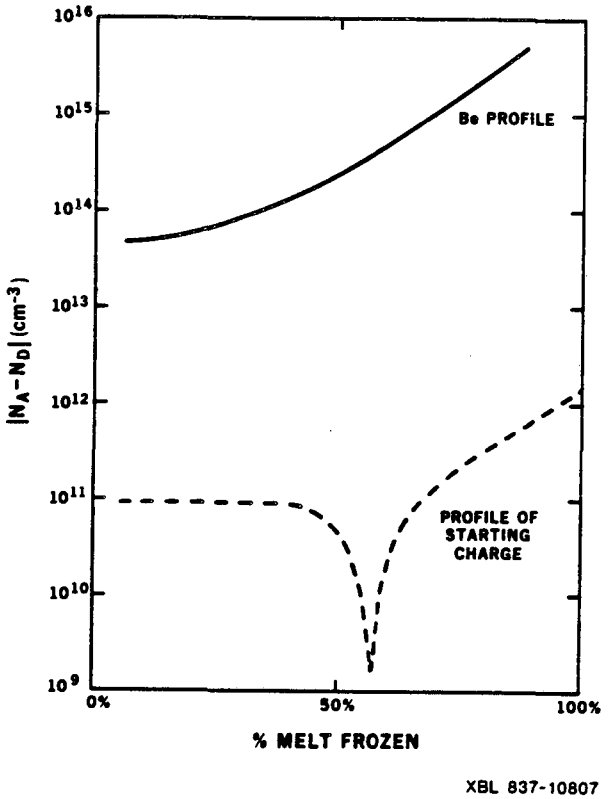

Fig. 25. Required Be and net shallow level concentrations for precise compensation of shallow levels in a Ge:Be detectors.

3.5 Comparison of Ge:Be and Ge:Ga Detector Performance at 42 μm

The most immediate application of Ge:Be detectors would be to provide increased sensitivity in the 30 - 50 μm wavelength range. As previously discussed, the responsivity and NEP of Ge:Ga detectors decrease and increase respectively as the photon energy increases beyond the peak of the spectral response at 90 μm. This trend is illustrated by Fig. 26, which shows the performance of a Ge:Ga photoconductor at successively shorter wavelengths of 93, 42, and 36 μm. Because the background flux varied for the different filter trains, the NEP data is presented as a ratio of NEP to $NEP_{(background\ limited)}$. The responsivity is presented in the dimensionless

quantity $G\eta$ so that a direct comparison at different photon energies is valid.

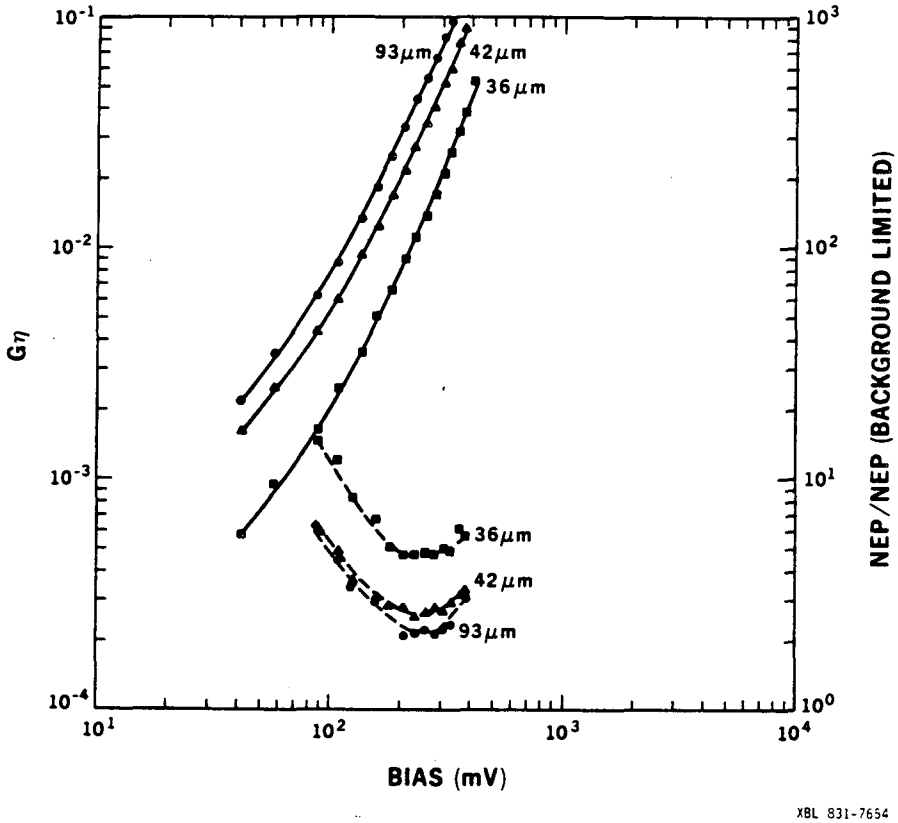

Fig. 26. Responsivity and NEP as a function of bias. T = 3.0 K, chopping frequency = 20 Hz. Solid lines indicate responsivity. Dashed lines indicate NEP.

Figure 27 compares the responsivity and NEP at 42 μm for a Ge:Be and Ge:Ga detector, each operated at its optimum temperature. The Ge:Ga detector ([Ga] = 2 x 10^{14} cm^{-3}, $[N_D]$ = 1 x 10^{12} cm^{-3}) was one of a number of state-of-the-art Ge:Ga detectors evaluated as part of a NASA project to characterize detectors produced from a number of commercially available materials[32]. This shows that Ge:Be detectors can provide higher responsivity and lower NEP at this wavelength than the best Ge:Ga detectors available today. Ge:Be detectors are less

limited by amplifier noise at low bias due to the higher responsivity and can be operated at higher bias since the breakdown bias is larger than in Ge:Ga. In addition, Ge:Be detectors are significantly less affected by the current spiking behavior which is common in Ge:Ga devices. Detectors operated at 3.8 and 4.2 K do not display any spiking behavior throughout the operating bias range. At 3.0 K, spiking occurs only very close to the breakdown field and does not extend to lower biases where the optimum NEP is attained.

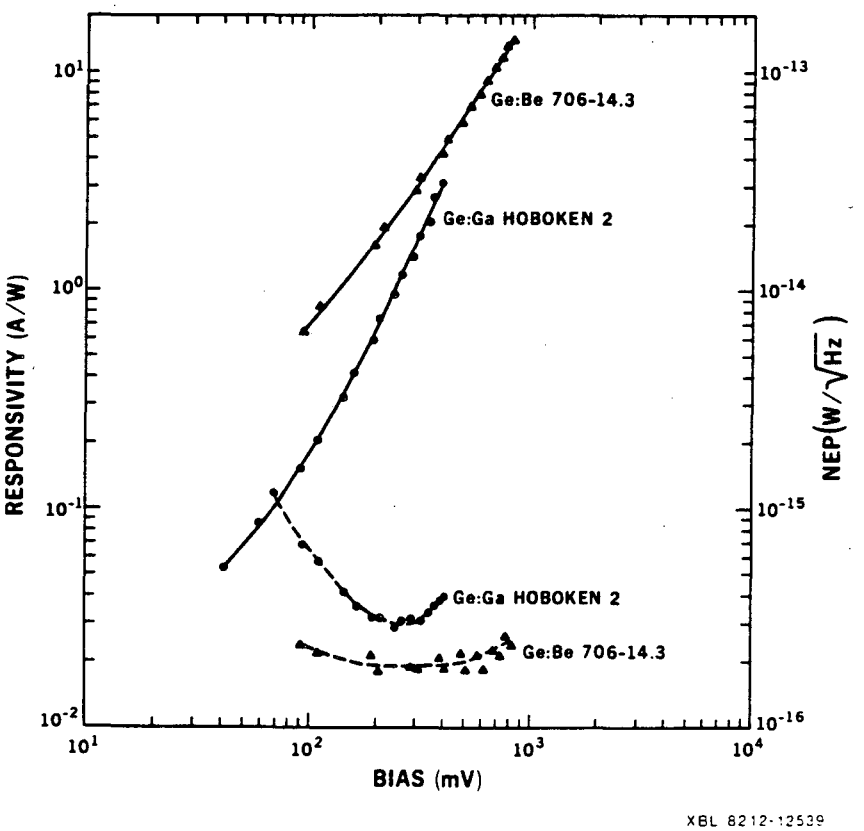

Fig. 27. Comparison of Ge:Be and Ge:Ga performance at 42 μm. T(Ge:Be) = 3.8 K, T(Ge:Ga) = 3.0 K, chopping frequency = 20 Hz. Solid lines indicate responsivity. Dashed lines indicate NEP. $NEP_{back.lim.} = 1.15 \times 10^{-16}$ W/ Hz.

4. Ge:Ga PHOTOCONDUCTOR DEVELOPMENT

4.1 Background

Ge:Ga photoconductors are presently used as detectors in the 30 - 120 μm range. Gallium is a Group III shallow acceptor in Ge ($E_{ionization}$ = 11 meV), and its behavior in the lattice is well described by the effective mass theory. The peak of the spectral response for Ge:Ga occurs at approximately 90 μm. The threshold wavelength for photoionization is ~ 125 μm.

The early choice of Ga as a dopant species for these long wavelength photoconductors was dictated primarily by the availability of material. Before the advent of high-purity Ge, Ge:Ga was used as the starting material for large-volume Li-drifted nuclear radiation detectors. Ga is a preferred dopant because its introduction into the crystal can be easily controlled. It is not a common contaminant in the crystal growth environment, and its small segregation coefficient (K = .087) makes it easy to remove from the starting charge. The Ge:Ga detectors evaluated in this study were fabricated from Czochralski-grown Ge. Ga doping was achieved by using a heavily-doped Ge:Ga master alloy.

A large amount of work has been done on the evaluation of Ge:Ga detectors prepared from standard, commercially available materials with [Ga] ~ 2×10^{14} cm^{-3} and a compensating donor concentration in the range of 10^{12} cm^{-3}. These detectors are well developed, generally providing responsivities in the range of 10 to 20 A/W with NEPs within a factor of two or less of the background limited level, and have already been utilized in space astronomy applications[33].

Research has continued, however, with the goal of providing a better fundamental understanding of extrinsic photoconductivity in Ge. A recent Ph.D. thesis completed by M. R. Hueschen, Physics Department, U.C. Berkeley, has characterized the behavior of several Ge:Ga photoconductors, with emphasis on how compensation and other variables such as temperature and applied field affect the carrier lifetime and mobility[34]. This has provided the background required for the work described here.

Hueschen used photoconductivity and photo-Hall effect measurements to study the behavior of low compensation Ge:Ga ($N_D \sim 10^{12}$ cm^{-3}) and ultra-low compensation Ge:Ga ($N_D \sim 10^{10}$ cm^{-3}). The ultra-low compensation Ge:Ga was grown at Lawrence Berkeley Laboratory, using the high-purity Ge growth facility. The low compensation Ge:Ga was single crystal material which had been grown earlier at LBL for Li-drifted radiation detectors. Hueschen found that the reduction in compensation resulted in longer lifetimes and higher mobilities, as would be expected with a reduction in ionized impurity sites.

Responsivities in the ultra-low compensation material were reported to be a factor of 10 times higher than the standard material. The increase in mobility and lifetime, however, caused these detectors to undergo impact ionization breakdown at very low bias voltages (1 V/cm as opposed to 3 - 4 V/cm in standard material). As a result, the optimum responsivity which could be attained with the ultra-low compensation material did not exceed that attained with the standard material. Hueschen's work indicated therefore that the degree of compensation greatly affects detector behavior and that very large reponsivities

could be obtained with ultra-low compensation. Further materials development was needed, however, to make detectors which could effectively utilize this increased responsivity and provide better performance in terms of responsivity than the detectors currently in use.

In order to provide a starting point for the continued evaluation and development of ultra-low compensation detector material, detectors from low compensation (112-15.8) and ultra-low compensation (583-4.6) crystals were evaluated. The results are presented in Fig. 28. These results corroborate Hueschen's results in all the major features. For the ultra-low compensation material, the responsivity at a given bias is approximately an order of magnitude larger, breakdown occurs at ~ 1 V/cm, and the lowest reported NEP is a factor of two above the best values obtained with the low compensation material. Hueschen reported background limited results for the latter material, with the ultra-low compensation material giving optimum NEPs a factor of two higher. Discrepancies in absolute values for NEPs are a common problem in low background photoconductor evaluation. The reasons for the variations are not fully understood, although the primary problem is to obtain an accurate estimate of the photon signal. It should be noted that all the results presented here were obtained with narrow band filtering, while a large number of other investigators use broad band illumination and consider an integrated response.

Hueschen established that the increased lifetime, due to the reduction in the number of ionized acceptor sites, made the primary contribution to the increased responsivity observed in the crystal #583 material. Increased mobility also contributed to the increased responsivity and low breakdown field. With a higher mobility, a

carrier can pick up more energy from a given field in a given lifetime ($V \alpha \mu E$) and attain the kinetic energy required for impact ionization at a lower applied field. The objective of this work has been to add neutral scatterers to the ultra-low compensation material and attempt to extend the operating bias range without creating additional charged centers which would act as recombination sites and decrease the lifetime.

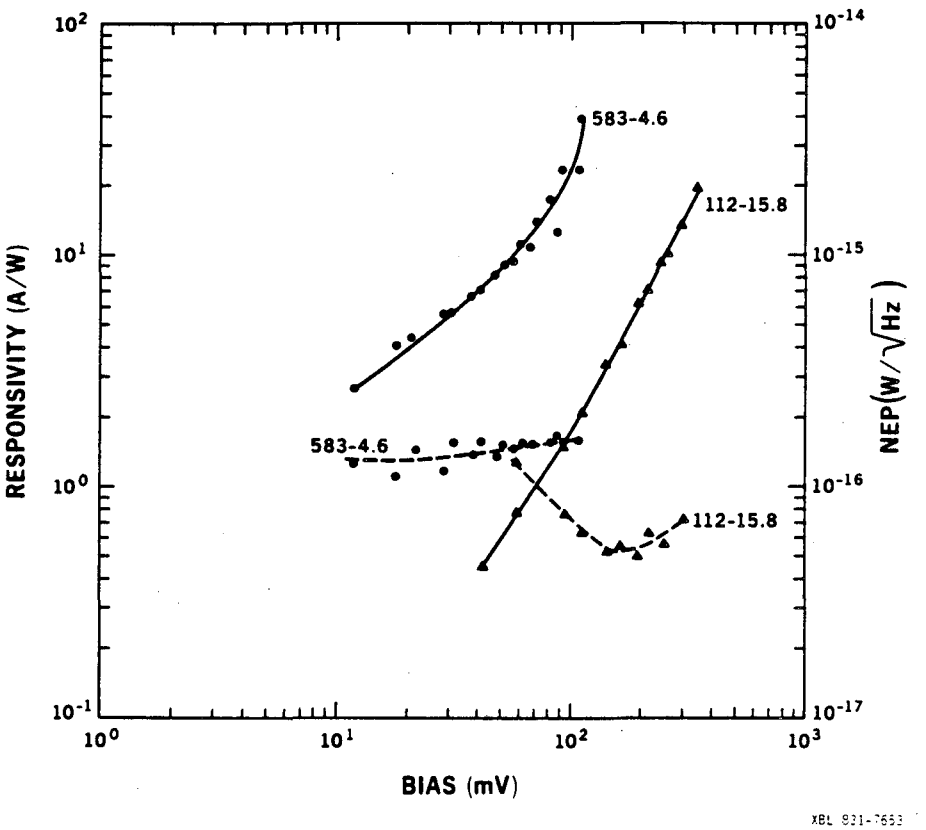

Fig. 28. Responsivity and NEP as a function of bias for low and ultra-low compensation Ge:Ga. T = 3.0 K, chopping frequency = 20 Hz. $NEP_{back.lim.} = 3.0 \times 10^{-17}$ W/ $\sqrt{Hz}$.

4.2 Detectors with Increased Ga Concentration

An initial attempt was made to provide increased scattering by increasing the concentration of Ga in the material. At T = 3 K, the optimum operating temperature for Ge:Ga devices, thermal generation from the 11 meV level is negligible, and the additional Ga should provide neutral impurity scattering. An ultra-low compensation Ge:Ga detector with [Ga] = 10^{15} cm^{-3} (crystal #582) was evaluated at 93 μm. Responsivity and NEP values as a function of bias are presented in Fig. 29.

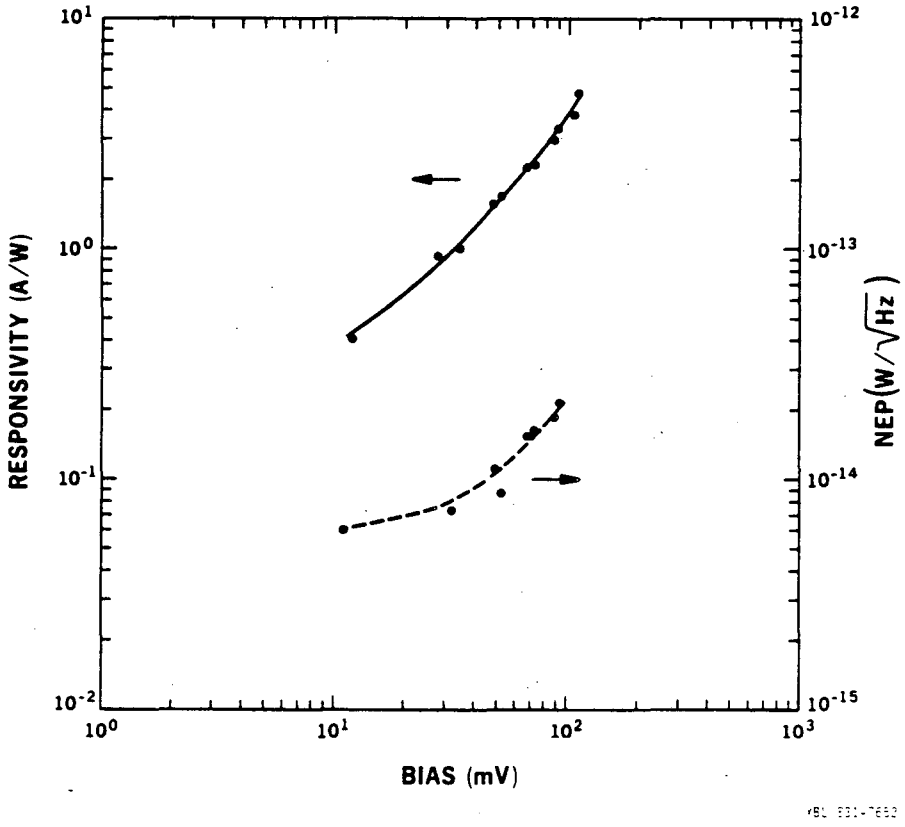

Fig. 29. Responsivity and NEP as a function of bias for Ge:Ga 582. T = 3.0 K, chopping frequency = 20 Hz. $NEP_{back.lim.}$ = 3.5 x 10^{-17} W/ $\sqrt{Hz}$.

The most obvious change that resulted from the increase in Ga concentration was an order of magnitude increase in the NEP. The

reason for this poor performance is best illustrated by considering the plot of thermal current versus applied field for the ultra-low compensation detectors with [Ga] = 2 x 10^{14} and 1 x 10^{15} cm^{-3} respectively (Fig. 30). At 4.2 K, the current through both detectors is of approximately equal value, indicating that the increased number of thermally ionized carriers ($p \sim N_A e^{-E}/kT$) in the more heavily doped sample is offset by a decreased mobility. The significant fact is that, as the temperature is decreased from 4.2 to 3.0 K, the thermally produced current in this detector does not decrease by the factor which would be predicted by the ratio of thermal ionization probabilities. Therefore, one concludes that a conduction mechanism which is either temperature independent or only weakly temperature dependent, such as hopping, plays a significant role in the more heavily doped detector. A similar result was observed for Ge:Be when the beryllium concentration exceeded 2 x 10^{15} cm^{-3}. High NEP values and a temperature insensitive thermal current were also characteristic of that case.

A second detector was carefully fabricated, etched, and tested in order to eliminate any question of possible surface contamination and conduction, or any other fabrication or mounting error which could cause this type of result. The second detector gave the same results.

These results indicate that a Ga concentration of 10^{15} cm^{-3} exceeds the limiting concentration imposed by the onset of hopping, even with a compensation as low as 10^{-4}. The results in Fig. 29 also indicate that the breakdown voltage was not changed significantly by increasing the Ga concentration a factor of five. This means that it would not be worthwhile to fabricate detectors with Ga concentrations between 2 x 10^{14}

and 1 x 10^{15} cm^{-3} in the hope of avoiding the significant hopping conduction. It does not appear, therefore, that an increase in the Ga concentration can be used to provide the additional scattering required in ultra-low compensation material without deleteriously affecting the conduction mechanism in the photoconductor.

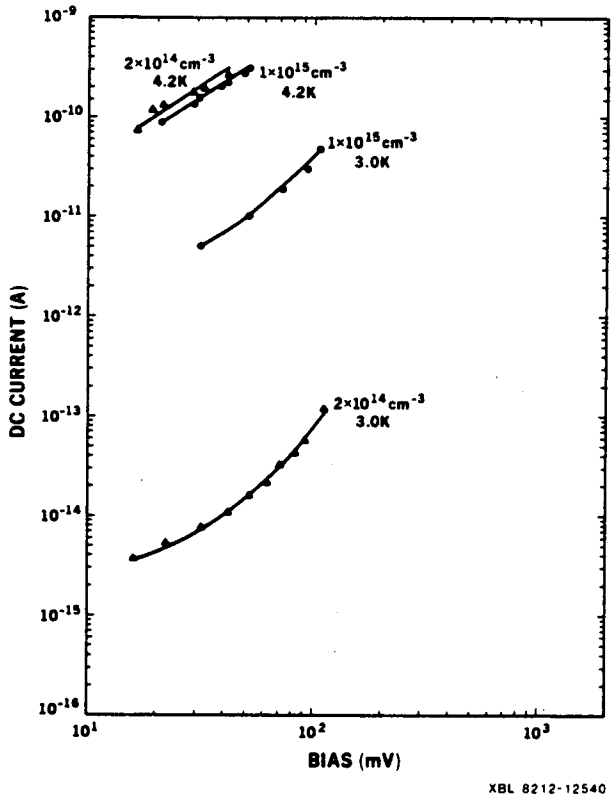

Fig. 30. Dark current as a function of bias at 4.2 and 3.0 K.

4.3 Ge:Ga:Cu Detector Performance

Decreased mobility in ultra-low compensation Ge:Ga can also be obtained by the introduction of neutral scatterers which do not play a role in conduction. A dopant such as Si or Sn, for example, could be added to the melt from which the Ge:Ga crystal is grown. In their

substitutional sites, these impurities are isoelectronic, but their distortion of the Ge lattice should lead to scattering and a decreased mobility. A second option is to introduce an electrically active dopant which may produce a semi-deep or deep level but is neutral at the temperatures at which the detector will be operated. Hopping conduction or the overlap of wavefunctions which leads to banding are less of a problem for impurities with larger binding energies since the radius of the wavefunction probability distribution is correspondingly decreased.

Copper was selected as a neutral scattering species because it can be easily introduced into the Ge:Ga material via high temperature diffusion. Copper is an interstitial diffuser and a triple acceptor in Ge with a first ionization energy of 44 meV. The solid solubility of Cu in Ge as a function of temperature has been determined by measuring the electrical activity after a diffusion and quenching process[35,36].

A 1 mm thick slice of ultra-low compensation Ge:Ga ([Ga] = 2 x 10^{14} cm^{-3}) was electroplated in a CuCN solution with a current of 20 mA for seven minutes. Copper was diffused into the sample for one hour at 600°C. The sample was removed from the furnace and air-cooled. The B contacts were implanted and then the slice was reheated to 600°C to dissolve the Cu precipitates. The sample was quenched directly into ethylene glycol. Titanium and Au layers were then deposited by Ar sputtering. The metal layers could not be thermally stress relieved since any low temperature thermal treatment would cause precipitation of the Cu. The solubility of Cu in Ge at 600°C is ~ 2 x 10^{14} cm^{-3}, so a concentration of neutral scatterers equal to or less than the concentration of Ga was introduced.

The comparison between a Cu-doped, ultra-low compensation Ge:Ga detector and a standard Ge:Ga detector ([Ga] = 2 x 10^{14} cm^{-3}, $[N_D] = 10^{12}$ cm^{-3}) is shown in Fig. 31. The scattering effect from the Cu has extended the operating bias range from 100 mV to ~ 200 mV. The responsivity of the Ge:Ga:Cu detector is higher at a given bias, and a comparable minimum NEP has been attained.

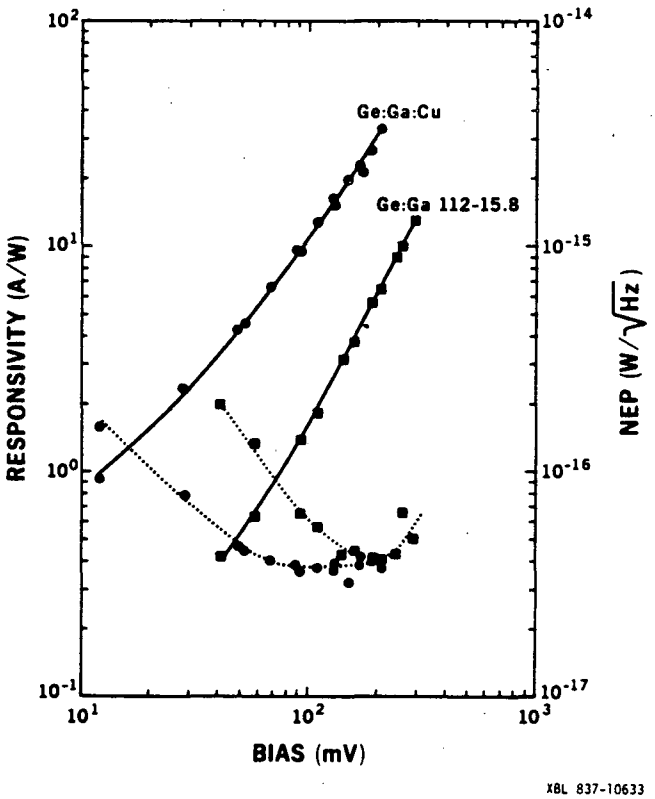

Fig. 31. Responsivity and NEP as a function of bias. T = 3.0 K. Chopping frequency = 20 Hz. Solid lines indicate responsivity. Dashed lines indicate NEP. $NEP_{back.lim.} = 2.2 \times 10^{-17}$ W/$\sqrt{Hz}$.

These results indicate that the addition of neutral scatterers may be effective in producing a high responsivity Ge:Ga detector from ultra-low compensation material. Future work should include a study of breakdown field as a function of Cu concentration to determine the optimum Cu concentration. A limitation on the production of these detectors is that the severe quench often cracks the Ge and small pieces must be selected for the devices. Microcracks or other quenched-in structural defects may also be contributing to the reduced mobility in the Cu-doped detectors. To separate this effect, the neutral scatterers could be added to the crystal by doping in the melt, and photoconductors produced from this material could be evaluated and compared to those produced by the diffusion method.

5. SUMMARY AND CONCLUSIONS

Ge:Be and Ge:Ga single crystal material has been developed for use as far-infrared photoconductors. Photoconductors have been evaluated under low photon background conditions using cooled electronics and narrow band filtering of an externally chopped signal. Detector responsivity and NEP have been determined as a function of bias, temperature, and materials parameters such as dopant concentration and compensation. The conclusions can be summarized as follows:

Ge:Be

- Ge:Be detectors provide higher responsivity and lower NEP at 42 μm than current state-of-the-art Ge:Ga detectors.
- Reliably doped Ge:Be with low dislocation density ($< 1000\ cm^{-2}$) has been produced using Czochralski growth from a carbon susceptor under vacuum. Measurable loss of Be to formation of BeO is avoided with these growth conditions.
- Variable temperature Hall effect measurements show that Be doped crystals grown from a high purity charge in a carbon susceptor have a net concentration of shallow acceptors.
- Optimum Be concentration was determined to be in the range of $5 \times 10^{14} - 1 \times 10^{15}\ cm^{-3}$. Hopping conduction was observed in detectors with $[Be] = 3.5 \times 10^{15}\ cm^{-3}$.
- Detectors in which the shallow acceptors are fully compensated have an impedance greater than $10^{11}\Omega$ at 4.2 K. Elimination of thermal currents in cases where $N_{D(shallow)} > N_{A(shallow)}$ should lead to an optimized Ge:Be detector.

- A strong temperature dependence of the responsivity was observed between 3.0 and 4.2 K in several detectors. This is due to an increase in lifetime caused by the temperature dependent probability of recombination into ionized shallow acceptor sites. This behavior is only observed if the shallow levels are closely compensated.
- Responsivities as high as G_η = .93 have been achieved at 4.2 K. Optimum detective quantum efficiencies of 46% have been attained at 3.8 K.
- The insensitivity of the NEP to temperature over the range of 2.5 - 4.2 K indicates that Ge:Be detectors can give excellent performance over a wide temperature range and could be easily integrated with other devices.

Ge:Ga

- Evaluation of a Ge:Ga detector with narrow band filtering at 93, 42, and 36 μm confirms the expected decreases in responsivity and detective quantum efficiency with increasing photon energy.
- Detectors produced from ultra-low compensation Ge:Ga ($N_D = 10^{10}$ cm^{-3}) with [Ge] = 10^{15} cm^{-3} exhibit decreased impedance due to hopping conduction.
- The introduction of Cu as a neutral scatterer extends the operating bias range for ultra-low compensation Ge:Ga detectors at 3.0 K to ~ 200 mV/mm. These detectors exhibit higher responsivity and comparable NEP than the undoped Ge:Ga.

REFERENCES

1. See, for example, "Proc. of the 1961 International Conference on Photoconductivity", Phys. and Chem. of Solids 22 (1961).

2. Anderson W W, Solid State Electron. 18, 235 (1975).

3. Bube R H, Photoconductivity in Solids (New York: John Wiley and Sons, Inc.) 58, 1960.

4. Brown D M and Bray R, Phys. Rev. 127, No. 5, 1593 (1962).

5. Bratt P R, "Impurity Germanium and Silicon Infrared Detectors", in: Semiconductors and Semimetals, Willardson R K and Beer A C, eds. (New York: Academic Press) Vol. 12, 67-71, 1977.

6. Keyes R J and Quist T M, "Low-Level Coherent/Incoherent Detection in the Infrared", in: Semiconductors and Semimetals, Willardson R K and Beer A C, eds. (New York: Academic Press) Vol. 5, 322-328, 1970.

7. Watson D M, Ph.D. thesis, University of California, Berkeley, 1982.

8. Present address: Downs Laboratory of Physics, California Institute of Technology, Pasadena, CA.

9. Low F J, SPIE 280, 56 (1981).

10. Haller E E, Hueschen M R and Richards P L, J. Appl. Phys. 34, 495 (1979).

11. Cross J W, Ho L T, Ramdas A K, Sauer R and Haller E E, "Excitation spectra of group II acceptors in Ge: Ge(Be°), Ge(Be^{-}) and Ge(Mg°)", to be published in Phys. Rev. B.

12. Shenker H, Swiggard E M and Moore W J, Trans. Met. Soc. AIME 239, 347 (1967).

13. Bratt P R, Lewis N N and Long L E, Final Technical Report NAS2-9385 (1977).

14. Brunsmann U, Egle H, Frenzl O and Dinges P, Final Report, ESTEC Contract 4458/80/NL/HP(SC) (1982).

15. Goncharov L A and Kervalishvili P D, Inorganic Materials 14, No. 6, 775 (1978).

16. Darken L S, IEEE Trans. Nucl. Sci. NS-26, No. 1, 324 (1979).

17. Sze S M and Irvin J C, Solid-State Electron. 11, 599 (1968).

18. Haller E E, Hansen W L and Goulding F S, Advances in Physics 30, No. 1, 93 (1981).

19. Hubbard G S, Haller E E and Hansen W L, IEEE Trans. Nucl. Sci. NS-26, No. 1, 362 (1978).

20. Van der Pauw L J, Phillips Res. Rpts. 13, 1 (1958).

21. Lee P A, Brit. J. Appl. Phys. 8, 340 (1957).

22. Blakemore J S, Phys. Rev. B 22, 743 (1980).

23. Fritzsche H and Lark-Horovitz K, Phys. Rev. 113, No. 4, 999 (1959).

24. Fritzsche H, "The Metal-Nonmetal Transition in Doped Semiconductors", in: The Metal-Nonmetal Transition in Disordered Systems, Friedman L R and Tunstall D P, eds. (Scottish Universities Summer School in Physics) 193, 1978.

25. Gershenzon E I, Gol'tsman G N and Mel'nikov A P, JETP Lett. 14, 185 (1971).

26. Haller E E, McMurray R E Jr., Falicov L M, Haegel N M and Hansen W L, to be published in Phys. Rev. Lett. Sept. 1983.

27. Lox M, Phys. Rev. 119, 1502 (1960).

28. Thomas R N, Braggins T T, Hobgood H M and Takei W J, J. Appl. Phys. 49, 2811 (1978).

29. Alexander D H, Baron R and Stafsudd O M, IEEE Trans. Elec. Dev. ED-27, No. 1, 71 (1980).

30. Geim K, Pensl G and Shultz M, Appl. Phys. A 27, 71 (1982).

31. Fritzsche H and Cuevas M, Phys. Rev. 119, 1238 (1960).

32. Haller E E, Haegel N M, Hansen W L and Luke P N, Final Report, NASA Contract No. W-14,606 (1982).

33. The Infrared Astronomical Satellite (IRAS) uses Ge:Ga for the 60 and 100 μm bands.

34. Hueschen M R, Ph.D. thesis, University of California, Berkeley, to be completed 1983.

35. Woodbury H H and Tyler W W, Phys. Rev. 105, 84 (1957).

36. Kitagawa H, Hashimoto K and Yoshida M, Jap. J. Appl. Phys. 21, 990 (1982).

37. Landsberg P T, Thermodynamics, (New York: Interscience Publishers) 274, 1961.

38. Fussel W B, NBS Technical Note 594-8 (1974).

39. Steel W H, De M and Bell J A, J. Opt. Soc. Am. 62, 1099 (1972).

APPENDIX SIGNAL CALCULATION AND DIFFRACTION ANALYSIS

Consider the following situation and ask: What is the DC photon flux of the blackbody sources and what is the chopped signal that the detector?

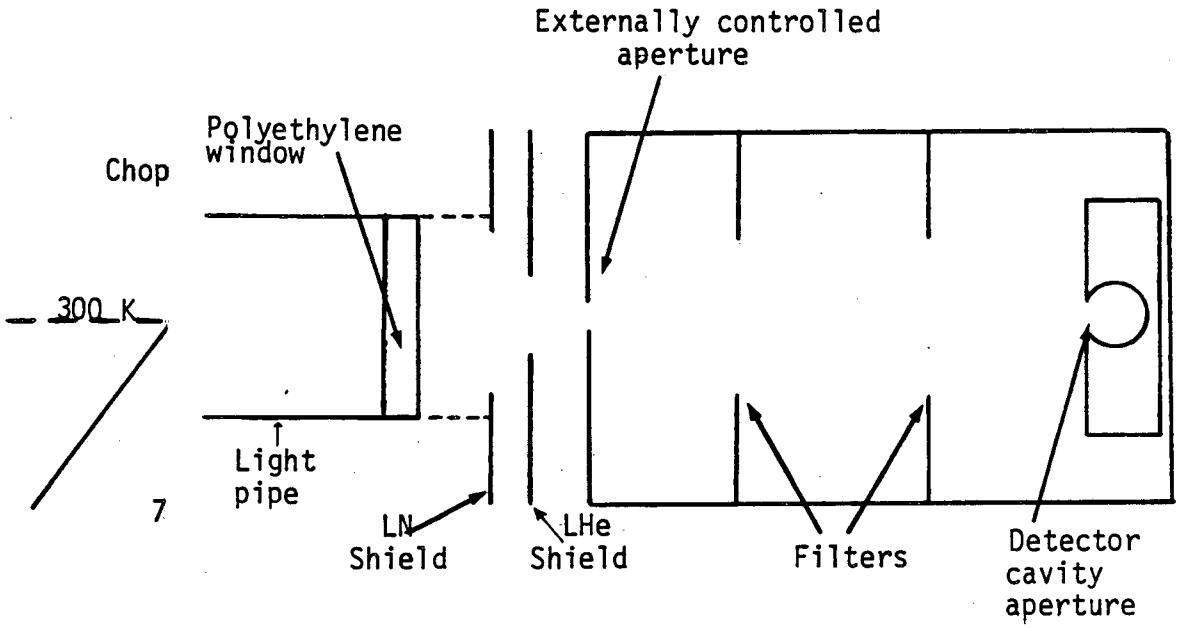

1) the blackbody radiation from the 300 and 77 K sources.

$$= \frac{2\pi hc^2}{\lambda^5}\left[\frac{hc}{e^{\lambda kT}} - 1\right]^{-1} \qquad 37$$

$$= \frac{3.74\times10^4}{\lambda^5}\left[e^{\frac{1.44\times10^4}{\lambda T}} - 1\right]^{-1} \qquad \text{for } \lambda(\mu m),\ T(K) \rightarrow W \text{ in Watts/cm}^2/\mu m$$

2) the transmission of the window experimentally.

ssmission measured through the window material.

Given $R + A + T = 1$ and $A \simeq E$.

For polyethylene $n = 1.46$ through far-IR

Since $\epsilon' = n^2 - k^2$, $\epsilon' \approx 2.1 - 2.5 \rightarrow k$ is small

$$R = \rho^2 = \left(\frac{n-1}{n+1}\right)^2 = 3\%$$

where R = reflectivity

T = transmissivity

E = emissivity

A = absorptivity

∴ Neglect R and $A + T = 1$ determines T and E.

3) Calculate the geometric factor, considering purely geometric optics.

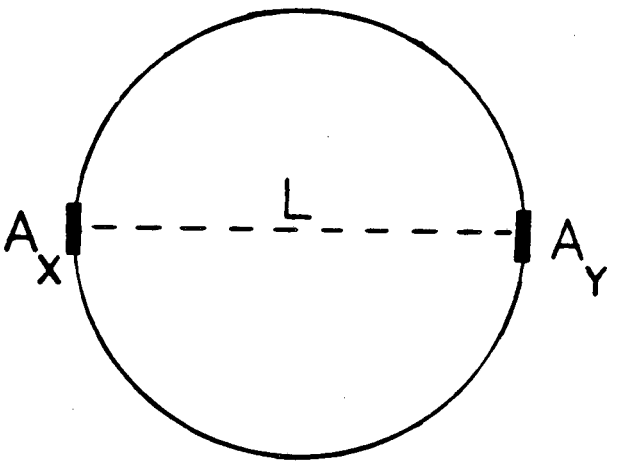

The radiation seen at y due to the source at x is:

$$W_{total} \times \frac{A_x A_y}{\pi L^2}$$

for W in watts/cm^2/μm and A_X, A_Y in cm^2, L in cm.

4) The filter trains have characteristic peak transmissions and bandwidths[7] (see Table 1).

T – transmission (peak) in %

Bandwidth (in μm)

5) Estimate diffraction losses[38]. With reference to Steel et al[39] (Diffraction Corrections in Radiometry), we consider the following:

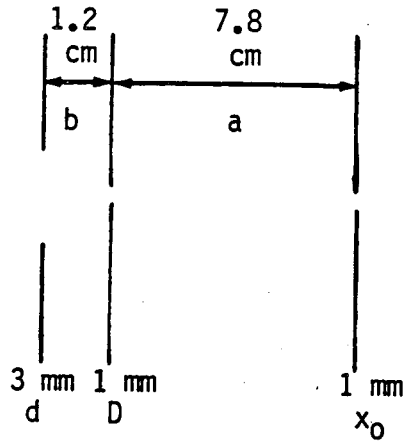

The diffraction loss can be estimated as:

$$\bar{E}(u,v,w_o) = (2\pi w_o)^{-1} \text{ Ln} \left[\frac{(v + w_o)^2 - u^2}{(v - w_o)^2 - u^2} \right]$$

where $u = \pi D^2(a^{-1} + b^{-1})(2\lambda)^{-1}$; $v = \pi Dd(2b\lambda)^{-1}$; and $w_o = \pi Dx_o(a\lambda)^{-1}$. The following results are obtained for the relevant geometry:

$\lambda(\mu m)$	$\bar{E}$(% Diffraction Loss)
93	18.1
42	8.1

6) Now the flux at the detector can be calculated. For the LN blackbody:

$$\text{Flux} = [W_{77} \times \text{window transmission} + W_{300} \times \text{window emissivity}]$$

$$\times \frac{A_1 A_2}{\pi L^2} \times \text{Filter transmission} \times \text{Bandwidth} \times \text{Diffraction loss}$$

For the 300 K blackbody:

$$\text{Flux} = W_{300} \times \frac{A_1 A_2}{\pi L^2} \times \text{Filter transmission} \times \text{Bandwidth} \times \text{Diffraction loss}$$

7) Calculate the signal.

Signal (p-p) = $\text{Flux}_{300} - \text{Flux}_{77}$ in W or photons/sec

Signal (rms) = Signal p-p/2.2 where 2.2 is the conversion to r.m.s for a square wave.

8) The background limited NEP can now be calculated.

$$NEP_{BLIP} = 2\sqrt{Ph\nu} \text{ in } W/\sqrt{Hz}; \text{ for } \eta = 1 \text{ and } P = \text{background power.}$$

The Bose-Einstein factor cannot always be neglected, so:

$$NEP_{BLIP} = \frac{2}{\left(1 - e^{-h\nu/kT_B}\right)} \sqrt{Ph\nu}$$

9) For the 42 μm (Ge:Be) and 93 μm (Ge:Ga) cases, the results are summarized below.

	42 μm	93 μm
W_{77}	3.34×10^{-6} W/cm^2/μm	8.26×10^{-7} W/cm^2/μm
W_{300}	1.26×10^{-4} W/cm^2 μm	7.90×10^{-6} W/cm^2/μm
Window Trans.	.85	.89
Emissivity	.15	.11
Geometric factor	3.2×10^{-7}cm^2	3.2×10^{-7}cm^2
Filter transmission	.13	.27
Bandwidth	.788 μm	1.045 μm
Diffraction loss	.08	.18
LN flux	7.13×10^{-13} W	1.21×10^{-13} W

(continued)	42 μm	93 μm
300 K flux	4.13×10^{-12} W	5.83×10^{-13} W
Signal (rms)	1.55×10^{-12} W	2.10×10^{-13} W
Signal (p-p)	3.42×10^{-12} W	4.64×10^{-13} W
Bose-Einstein factor	.99	.865
$NEP_{background\ limited}$	1.15×10^{-16} W/$\sqrt{Hz}$	3.45×10^{-17} W/$\sqrt{Hz}$

APPENDIX 2 - THERMODYNAMICS CALCULATIONS FOR BeO FORMATION

Thermodynamics calculations based on the free energy of formation and the mass action law can give an indication of the stability of an oxide under various conditions of temperature, concentration, and environment. The following are basic calculations which were used as guidelines for selecting appropriate conditions for Czochralski growth of Be-doped germanium.

1) Free energy of formation of BeO.

The free energy of formation for a reaction is often modeled by the equation:

$$\Delta G = \Delta H^{o} - T\Delta S \qquad \Delta G \equiv \Delta F \tag{1}$$

where ΔH and ΔS are considered temperature independent. For the formation of BeO:

$$Be + \frac{1}{2} O_2 \rightarrow BeO \tag{2}$$

$\Delta H = -143{,}000$ cal. and $\Delta S = 23$ cal.

Placing this relation on an Ellingham diagram, one sees that BeO is a very stable oxide. Under equilibrium conditions, Be would reduce any of the oxides whose ΔF curves lie above ΔF_{BeO} at a given temperature.

2) BeO formation under H_2.

In a germanium melt, it is necessary to consider the solution thermodynamics of a small concentration of Be in a germanium solvent. This approach was taken by Darken and applied to the stability of oxides in high-purity Ge crystal growth[16].

The question of interest is whether a Be-doped crystal can be grown under a H_2 atmosphere without major precipitation of BeO in the melt. Because the H_2 atmosphere will contain a certain amount

of H_2O, the reaction to be considered is:

$$Be + H_2O \rightarrow BeO + H_2. \qquad (3)$$

By the mass action law:

$$K = \frac{P_{H_2}}{P_{H_2O}} \left(\frac{1}{a_{Be}}\right) \qquad (4)$$

and

$$\log K = \frac{-\Delta G^\circ}{2.303\ RT} \qquad (5)$$

where $a_{BeO} = 1$; $a_{Be} = \gamma N$; and N = mole fraction.
The activity coefficient, γ, is difficult to determine. Therefore, Darken assumes $\gamma = 1$ (the ideal case). Applying these two equations, he concludes that the maximum Be concentration allowed prior to the formation of stable BeO is 2.8×10^{14} cm^{-3} for crystal growth at 1200 K with $p(H_2)/p(H_2O) = 10^5$.

For current photoconductor work, we are interested in Be concentration of 5×10^{14} cm^{-3}. To analyze the extreme case, we consider what limiting partial pressure ratio would be required to prevent oxide formation for a concentration of 5×10^{15} cm^{-3}. The ΔG° value of -72,400 is taken directly from Darken's calculations, but this data is available in standard thermodynamics tables.

Applying Equations 4 and 5, we obtain:

$$\log K = \frac{72{,}400}{2.303(1.987)(1200)} = 13.2$$

$$K = 1.58 \times 10^{13}$$

$$K = \frac{P_{H_2}}{P_{H_2O}} \times \frac{1}{a_{Be}} = \frac{P_{H_2}}{P_{H_2O}} \left(\frac{1}{N_{Be}}\right) \qquad \gamma = 1$$

$$1.58 \times 10^{13} = \frac{1}{N}\left(\frac{P_{H_2}}{P_{H_2O}}\right)$$

Concentration = 5×10^{15} ⇒ Molality = 1.56×10^{-6} ⇒ Mole Fraction = 1.13×10^{-7}

$$1.58 \times 10^{13} = \frac{1}{1.13 \times 10^{-7}}\left(\frac{P_{H_2}}{P_{H_2O}}\right)$$

$$\frac{P_{H_2}}{P_{H_2O}} = 1.8 \times 10^{6}$$

$$\frac{P_{H_2O}}{P_{H_2}} = 5.6 \times 10^{-7}$$

Since the usual ratio of H_2O/H_2 partial pressures attained during crystal growth under H_2 is ~ 10^{-5}, the atmosphere used for high purity growth is unsuitable for growing Be-doped crystals for photoconductor applications because the formation of BeO is thermodynamically favorable. Based on this conclusion, all Ge:Be crystals were grown under vacuum.

APPENDIX 3 - TEMPERATURE DEPENDENCE OF THE RESPONSIVITY IN MULTI-LEVEL EXTRINSIC DETECTORS

The equations presented here have been taken directly from the theoretical model proposed by Alexander et al[29] and applied to the Ge:Be system as shown in Fig. 21.

Responsivity (in A/W) is proportional to the change in detector conductance with a change in photon flux. Assuming uniform radiation of a single wavelength (valid assumptions for the case of Ge:Be in an integrating cavity under narrow band illumination),

$$R(T) \propto \frac{d(1/R)}{dQ} \propto \mu(T) \frac{dp(T)}{dQ} \qquad (1)$$

where R = responsivity; μ = mobility; Q = background flux;
p = concentration of free holes.

The lifetime effect which leads to the strong temperature dependence is contained in the dp(T)/dQ term. To determine dp(T)/dQ as a function of temperature, the equilibrium expression for p is needed as a function of dopant concentrations, temperature, and photon flux.

From the charge neutrality equation:

$$p + N_D = \sum_i \frac{N_i}{\frac{g_i p}{p_{1i} + Q\sigma_i/C_i}}$$

N_i = acceptor concentration, cm^{-3}
p = free hole concentration, cm^{-3}
N_D = donor concentration, cm^{-3}
g = level degeneracy
p_{1i} = hole concentration when $E_F = Ei$

Q = photon flux density, $cm^{-2}s^{-1}$

σ = photon capture cross section, cm^2

C = recombination coefficient, cm^3s^{-1}.

For Ge:Be, under a photon flux of $\lambda = 42\ \mu$, one can make the following assumptions:

(1) N_D = the concentration of shallow residual donors (primarily P).

(2) The second ionization stage of the Be, Be^{--}, can be neglected.

(3) Shallow residual acceptors (primarily B and Al) obey the effective mass approximation, and can be considered as one level, N_A, with $E_A = 10$ meV.

Thus, for Ge:Be:

$$p + N_D = \frac{N_{Be}}{1 + \dfrac{g_{Be}\,p}{P_{1Be} + \dfrac{Q\sigma_{Be}}{C_{Be}}}} + \frac{N_A}{1 + \dfrac{g_A p}{P_{1A} + \dfrac{Q\sigma_A}{C_A}}} \tag{3}$$

An expression for $\frac{dp}{dQ}$ is obtained by solving (3) for p and differentiating.

$$\frac{dp}{dQ} = \frac{\left.\dfrac{Ngp\sigma/C}{\left(1 + \dfrac{gp}{P_1 + \frac{Q\sigma}{C}}\right)^2\left(P_1 + \frac{Q\sigma}{C}\right)^2}\right|_{Be} + \left.\dfrac{Ngp\sigma/C}{\left(1 + \dfrac{gp}{P_1 + \frac{Q\sigma}{C}}\right)^2\left(P_1 + \frac{Q\sigma}{C}\right)^2}\right|_{A}}{\left.\dfrac{Ng}{\left(1 + \dfrac{gp}{P_1 + \frac{Q\sigma}{C}}\right)^2\left(P_1 + \frac{Q\sigma}{C}\right)}\right|_{Be} + \left.\dfrac{Ng}{\left(1 + \dfrac{gp}{P_1 + \frac{Q\sigma}{C}}\right)^2\left(P_1 + \frac{Q\sigma}{C}\right)}\right|_{A}}$$

This equation can be solved by first solving (3) for p (using numerical iteration) and then solving directly for dp/dQ.

Alexander et al[29] consider the temperature dependence of dp/dQ in three regimes:

Regime	Assumptions	Result	Note
1) Occupation of all levels photon dominated	$p_1 \to 0$	$\frac{dp}{dQ} = \frac{N_{Be}\sigma_{Be}}{N_D g_{Be} C_{Be}}$	-Temperature independent
2) Occupation of N_A thermally dominated (overcompensated)	$p_{1A} >> \frac{Q\sigma_A}{C_A}$	$\frac{dp}{dQ} = \frac{N_{Be}\sigma_{Be}}{(N_D - N_A) g_{Be} C_{Be}}$	-Higher responsivity -Temperature independent
3) Occupation of N_A thermally dominated (undercompensated)	$p_{1A} >> \frac{Q\sigma_A}{C_A}$	$\frac{dp}{dQ} = \frac{N_{Be}\sigma_{Be}}{N_D g_{Be} C_{Be}} \frac{N_A}{(N_A - N_D)}$	-Higher responsivity -Temperature independent

The result for dp/dQ as a function of temperature is shown schematically below:

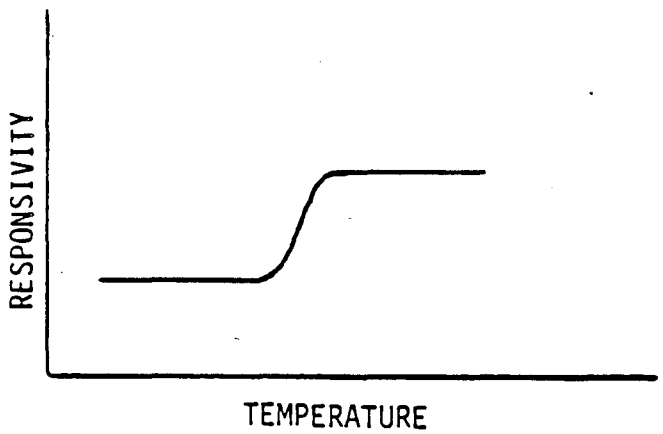

A series of plateaus (the number depending on the number of underlying levels) will be connected by regions of strong temperature dependence.

Finally, at high enough temperatures that the thermal ionization of the Be begins to exceed photo-ionization, the responsivity will decrease as:

$$\frac{dp}{dQ} = \frac{\sigma_{Be}}{C_{Be}} \quad \frac{N_{Be}}{N_v g_{Be}} \quad e^{\left(\frac{E_{Be}}{2kT}\right)}$$

TECHNICAL INFORMATION DEPARTMENT
LAWRENCE BERKELEY LABORATORY
UNIVERSITY OF CALIFORNIA
BERKELEY, CALIFORNIA 94720